Response to Reviewer #2:

Our apologies for missing comments 6 and 7 in our original response. (In converting the pdf to a word file we could copy from these were unintentionally lost by us.) We thank the reviewer for considering the revisions we have already made. Below we provide a response for both comments 6 and 7. Our responses are in **blue** and the initial reviewer comments in **black**.

1. Title should bear the word "laboratory" since the observed results might not be applicable to real world fires. For e.g., something like: "Laboratory-based biomass burning particles from a wide variety of fuels: Part 1: Properties of primary particles"

We understand the reviewers point here. However, we argue that there is nothing in the current title to indicate that these are "real-world" particles. (We assume by "real-world" the reviewer specifically means "ambient." The fires we sampled from were most assuredly "real.") In noting that the measurements are for "a wide variety of fuels" we believe it is implied that this is a laboratory experiment. Similarly, this is the case when we note the focus on "primary particles" as ambient studies have had limited success at accessing truly "primary" particles given the logistical challenges of getting close enough to fires and the rapid aging that occurs in the atmosphere. Instead of adjusting the title, we have updated the first sentence of the abstract to include the word "laboratory."

2. The authors provide no explanation (beyond a hand waving argument) to back the statement "The contribution of coating-induced enhancements (i.e. lensing effects) to absorption by black carbon are shown to be negligible for all conditions". Lensing or focusing of light to the core could also be possible with weakly light-absorbing coat- ing materials such as brown carbon with low imaginary index of refraction. Such a coating would facilitate lensing in addition to itself absorbing. One convincing way to declare that "no lensing" takes place is by looking at the internal field strength of a brown-carbon coated BC aggregate (see methodology in Chakrabarty and Heinson, Phys. Rev. Lett, 2018). I would like to see such a rigorous analysis performed (DDA or T-Matrix and not Mie-based core-shell) by the authors on a few BC aggregates coated with BrC vs non-refractory materials and convincing the reviewer and the community if indeed the "no lensing" claim is valid. If the authors cannot perform such an anal- ysis, then I suggest that they remove all statements from the abstract and the main text regarding "negligible coating-induced enhancements (lensing effects)". Instead, rephrase or replace the sentences with "brown carbon-coated BC particles yield ab- sorption enhancements of x and y values. . ."

This particular comment follows directly from the Reviewer's comment #3, questioning whether our conclusion that the "lensing" enhancement is "negligible." However, here the reviewer (i) asks for calculations including BrC and (ii) indicates that if we cannot do such calculations we should entirely revise the discussion of the absorption enhancement. We address the question of whether the lensing-induced absorption enhancement is "negligible" extensively in our original response to the Reviewer's comment #3. While we concluded that use of the "negligible" is justified, we have nonetheless revised the manuscript to indicate it as "minor". (We have additionally gone through now and done a search for "negligible," replacing it with "minor.") Here, we address more specifically the utility or appropriateness of inclusion of calculations such as those suggested. In short, we do not think that including results of such

calculations would add substantial value to the manuscript. One reason is that we do not have knowledge of the internal morphology of the BC-containing particles. Given this absence of knowledge, it would be necessary for us to perform systematic calculations over different particle geometries and coating amounts to glean insights. However, such calculations have already been performed by many researchers and results are available in the literature, both for non-absorbing and weakly absorbing coatings (Adachi et al., 2010;Kahnert and Devasthale, 2011;Kahnert et al., 2012;Liu et al., 2015;Kahnert, 2017;Liu et al., 2017a;Zhang et al., 2017;Kanngiesser and Kahnert, 2018;Zhang et al., 2018). Performing new calculations here is therefore, in our opinion, unnecessary. Instead, we believe it sufficient to point to the literature, which we have done by citing the relatively early work by Adachi et al. (2010), where it is demonstrated that non core-shell internal particle morphologies can lead to "lensing" enhancements notably smaller than the core-shell solution.

Further, we reiterate that we measure the mass-weighted mean coating-to-core ratio. The actual population of particles sampled have a diversity of coating-to-core ratios. As has been established previously (Cappa et al., 2012;Fierce et al., 2016;Liu et al., 2017b), when the actual diversity of coating-to-core ratios across the population is accounted for smaller enhancements are obtained compared to that obtained assuming all particles have the mean coating-to-core ratio. For particularly diverse populations of particles, the population-weighted enhancement can be substantially less than that obtained assuming the mean coating-to-core ratio for all particles (Fierce et al., 2016). Thus, a single, or even a "few" calculations for some arbitrary particle morphologies would not, in our opinion, be especially informative. Instead, it would be necessary to perform calculations over a wide range of assumed particle populations and assumed internal morphologies to capture the likely true behavior. Such an exercise is well-beyond the scope of this manuscript, which is predominately observational, and further challenged by the lack of specific information regarding the internal particle morphology or the distribution of coating thicknesses across the particle population. Yet, we can give two examples here to illustrate the general conclusions we are likely to reach should we perform such calculations. Example 1: Assume two 130 nm diameter BC particles. One has a coating-to-core ratio of zero (bare BC) while the other has a coating-to-core ratio of 20. The mean coating to core ratio is 10. The core-shell Mie enhancement for the first particle is 1 while for the second is 2.45. So, the mean enhancement is 1.72, notably lower than an enhancement of 2.1 if the coating-to-core ratio for both particles were 10. While this enhancement is still quite a bit larger than 1, this illustrates the point that consideration of particle diversity generally leads to reductions in the enhancement. Example 2: Assume a log normal distribution of BC cores (mode diameter = 120 nm, width = 1.6). Assume also that the coating amount decreases with core size, consistent with condensational growth, with an (arbitrary) functional form illustrated in the following figure. Set the coating thickness distribution such that the mean coating-to-core ratio is 5, a "thick" value typical of our observations. The resulting coating-induced enhancement is 1.35 for the distribution, compared to a value of 1.79 if all particles had the same coating coating-to-core ratio. Again, a substantial reduction is observed for the more diverse (variable coating-to-core ratio) population compared to the constant coating case. Other functional forms for the coating distribution can be chosen, which would give different—albeit consistent—results, reflecting the particular nature of the assumed distribution; this includes distributions that yield even smaller ensemble-average enhancements for the same coating-to-core ratio. We can include the results of calculations of this sort in the manuscript. However, we do not feel that they are appropriate here given that we do not know the coating distribution. Additionally, we note that we have

assumed a core-shell morphology here, which generally yields larger enhancements compared to more detailed calculations that account for internal particle morphology.

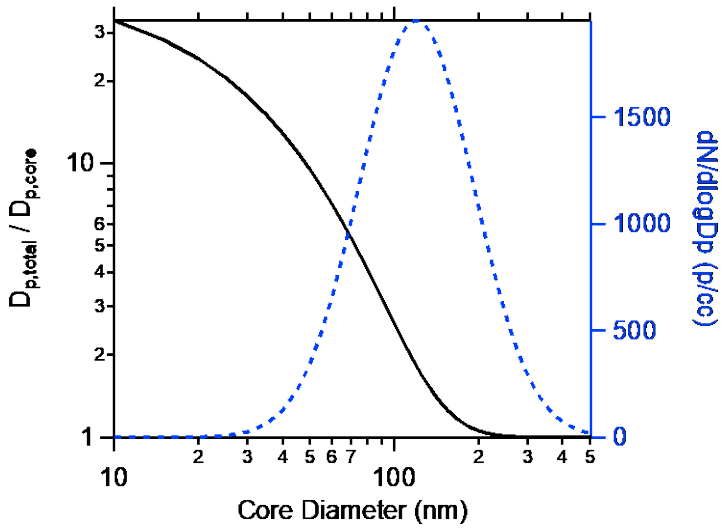

Ultimately, given what the literature says about the importance of considering both internal morphology and of particle populations we believe it is a reasonable inference (and not a "hand waving argument") to conclude that our observations point to the lensing-induced absorption enhancement being "negligible for all conditions." We further believe that citation of the existing literature is preferred over the addition of calculations here. Nonetheless, as noted above, we have revised the statements in the abstract and throughout the manuscript as follows to make clearer that (i) we refer to results from our experiments and (ii) that the effect is "minor" rather than "negligible." Specifically, for the abstract we have revised to state: "The contribution of coating-induced enhancements (i.e., "lensing" effects) to BC absorption are shown minor for all of the burns despite some burns producing particles have large ensemble-average coating-to-core mass ratios."

References:

Adachi, K., Chung, S. H., and Buseck, P. R.: Shapes of soot aerosol particles and implications for their effects on climate, J. Geophys. Res., 115, D15206, https://doi.org/10.1029/2009jd012868, 2010.

Cappa, C. D., Onasch, T. B., Massoli, P., Worsnop, D., Bates, T. S., Cross, E., Davidovits, P., Hakala, J., Hayden, K., Jobson, B. T., Kolesar, K. R., Lack, D. A., Lerner, B., Li, S. M., Mellon, D., Nuaanman, I., Olfert, J., Petaja, T., Quinn, P. K., Song, C., Subramanian, R., Williams, E. J., and Zaveri, R. A.: Radiative absorption enhancements due to the mixing state of atmospheric black carbon, Science, 337, 1078-1081, https://doi.org/10.1126/science.1223447, 2012.

Fierce, L., Bond, T. C., Bauer, S. E., Mena, F., and Riemer, N.: Black carbon absorption at the global scale is affected by particle-scale diversity in composition, Nat. Comm., 7, https://doi.org/10.1038/ncomms12361, 2016.

Kahnert, M., and Devasthale, A.: Black carbon fractal morphology and short-wave radiative impact: a modelling study, Atmospheric Chemistry and Physics, 11, 11745-11759, https://doi.org/10.5194/acp-11-11745-2011, 2011.

Kahnert, M., Nousiainen, T., Lindqvist, H., and Ebert, M.: Optical properties of light absorbing carbon aggregates mixed with sulfate: assessment of different model geometries for climate forcing calculations, Opt. Express, 20, 17, https://doi.org/10.1364/oe.20.010042, 2012.
Kahnert, M.: Optical properties of black carbon aerosols encapsulated in a shell of sulfate: comparison of the closed cell model with a coated aggregate model, Opt. Express, 25, 24579-24593, https://doi.org/10.1364/oe.25.024579, 2017.
Kanngiesser, F., and Kahnert, M.: Calculation of optical properties of light-absorbing carbon with weakly absorbing coating: A model with tunable transition from film-coating to spherical-shell coating, J. Quant. Spectrosc. Radiat. Transf., 216, 17-36, https://doi.org/10.1016/j.jqsrt.2018.05.014, 2018.
Liu, C., Li, J., Yin, Y., Zhu, B., and Feng, Q.: Optical properties of black carbon aggregates with non-absorptive coating, Journal of Quantitative Spectroscopy and Radiative Transfer, 187, 443-452, https://doi.org/10.1016/j.jqsrt.2016.10.023, 2017a.
Liu, D. T., Taylor, J. W., Young, D. E., Flynn, M. J., Coe, H., and Allan, J. D.: The effect of complex black carbon microphysics on the determination of the optical properties of brown carbon, Geophysical Research Letters, 42, 613-619, https://doi.org/10.1002/2014gl062443, 2015.
Liu, D. T., Whitehead, J., Alfarra, M. R., Reyes-Villegas, E., Spracklen, D. V., Reddington, C. L., Kong, S. F., Williams, P. I., Ting, Y. C., Haslett, S., Taylor, J. W., Flynn, M. J., Morgan, W. T., McFiggans, G., Coe, H., and Allan, J. D.: Black-carbon absorption enhancement in the atmosphere determined by particle mixing state, Nat. Geosci., 10, 184-U132, https://doi.org/10.1038/ngeo2901, 2017b.
Zhang, X., Mao, M., Yin, Y., and Wang, B.: Absorption enhancement of aged black carbon aerosols affected by their microphysics: A numerical investigation, Journal of Quantitative Spectroscopy and Radiative Transfer, 202, 90-97, https://doi.org/10.1016/j.jqsrt.2017.07.025, 2017.
Zhang, X., Mao, M., Yin, Y., and Wang, B.: Numerical Investigation on Absorption Enhancement of Black Carbon Aerosols Partially Coated With Nonabsorbing Organics, Journal of Geophysical Research: Atmospheres, 123, 1297-1308, https://doi.org/10.1002/2017jd027833, 2018.

Biomass-burning derived particles from a wide variety of fuels: Part 1: Properties of primary particles

Crystal D. McClure[1], Christopher Y. Lim[2,%], David H. Hagan[2], Jesse H. Kroll[2], Christopher D. Cappa[1,3,*]

[1] Department of Civil and Environmental Engineering, University of California, Davis, CA 95616
[2] Department of Civil and Environmental Engineering, Massachusetts Institute of Technology, Cambridge, MA, USA
[3] Atmospheric Sciences Graduate Group, University of California, Davis, CA, USA 95616
[%] Now at Department of Chemistry, University of Toronto, Ontario, Canada

[*] To whom correspondence should be addressed: cdcappa@ucdavis.edu

ABSTRACT

Relationships between various optical, physical, and chemical properties of biomass combustion derived particles are characterized for particles produced in the laboratory from a wide range of fuels and burn conditions. The modified combustion efficiency (MCE), commonly used to parameterize biomass particle emissions and properties, is shown to generally have weak predictive capabilities, especially for more efficient combustion conditions. There is, however, a strong relationship between many intensive optical properties (e.g. single scatter albedo, Ångstrom absorption exponent, mass absorption efficiency) and the organic aerosol-to-black carbon ([OA]/[BC]) mass ratio over a wider range than previously considered (0.3 to 10^5). The properties of brown carbon (BrC, i.e. light absorbing organic carbon) also vary with [OA]/[BC]. Coating-induced enhancements (i.e., "lensing" effects) contribute only a minor amount to BC absorption for all of the burns despite some burns producing particles having large ensemble-average coating-to-core mass ratios. The BC-OA mixing state varies strongly with [OA]/[BC]; the fraction of OA that is internally mixed with BC decreases with [OA]/[BC] while the relative amount of OA coated on BC increases. In contrast, there is little relationship between many OA bulk chemical properties and [OA]/[BC], with the O:C and H:C atomic ratios and the relative abundance of a key marker ion (m/z = 60, linked to levoglucosan) all showing no dependence on [OA]/[BC]. In contrast, both the organic nitrate fraction of OA and the OA volatility do depend on the [OA]/[BC]. Neither the total particle or BC-specific size distributions exhibit any clear dependence on the burn conditions or [OA]/[BC], although there is perhaps a dependence on fuel type. Overall, our results expand on

Deleted: The contribution of c

Deleted: by black carbon are shown to be negligible

Deleted: conditions

existing knowledge to contribute new understanding of the properties of particles emitted from biomass combustion.

1 Introduction

While it is understood that both open and controlled biomass combustion are major sources of particles to the atmosphere (Andreae and Merlet, 2001), questions remain regarding the properties of the emitted particles, their relationship with combustion conditions and fuel type, and their atmospheric evolution. Particles emitted from biomass combustion impact the global radiation budget and contribute to poor air quality in impacted regions. The emitted primary particles are primarily composed of organic aerosol (OA) and black carbon (BC), in varying amounts, with trace inorganic species (Reid et al., 2005;McMeeking et al., 2009;Levin et al., 2010). Particle intensive properties are often compared against the modified combustion efficiency (MCE ~ $\Delta[CO_2]/(\Delta[CO]+\Delta[CO_2])$), which provides a measure of the combustion efficiency of a burn. For example, various particle properties show some relationship with MCE, but often these relationships are weak, especially for more efficient combustion (higher MCE, corresponding typically to flaming conditions) (McMeeking et al., 2009;Liu et al., 2013;McMeeking et al., 2014). Understanding the diversity in the chemical, physical, and optical properties of the emitted particles is important for establishing the fire- or region-specific emissions and subsequent impacts.

The emitted OA from biomass combustion is somewhat light absorbing (Kirchstetter et al., 2004). Absorbing OA is commonly referred to as brown carbon (BrC), with properties that appear to depend on the fuel and combustion conditions (Saleh et al., 2014;Laskin et al., 2018), which affect particle organic composition (Jen et al., 2019). However, the properties of primary BrC absorption and, especially, understanding of the relationships between BrC absorption and other particle properties and burn conditions is only beginning to be unraveled. Additionally, it is established from theory and laboratory experiments that non-absorbing coatings on black carbon and other strongly absorbing particles can enhance the absorption (commonly referred to as the "lensing" effect but more accurately termed here the coating-induced enhancement) (Fuller et al., 1999;Bond et al., 2006;Lack et al., 2009;Shiraiwa et al., 2010;Cappa et al., 2012). Yet, the extent to which coating-induced enhancements impact absorption by ambient particles or for mixed-

component particles from complex sources, such as biomass burning, remains contentious (Cappa et al., 2012;Healy et al., 2015;Liu et al., 2015;Peng et al., 2016;Liu et al., 2017).

Here, we expand on current understanding of the relationships between various primary particle properties and burn conditions by analyzing measurements of primary biomass burning particles produced from combustion of a variety of fuel types, many of particular relevance to the western U.S.. We demonstrate that various optical properties exhibit a strong relationship with the [OA]/[BC] mass ratio, much stronger than their relationship with the MCE. We use the measurements to quantify the individual contributions of BC, BrC and from internal mixing of BC to the observed light absorption, and examine the variability in the properties of BrC specifically. We uniquely characterize the mixing state of BC and OA, and how mixing state vary between individual burns and depend on the mean properties of the emitted particles. We characterize the variability of OA-specific properties, including OA volatility, bulk chemical composition (characterized by the O:C and H:C atomic ratio, and the presence of key marker ions), and, uniquely, the relative abundance of organic nitrate species. We also examine the variability in the emitted particle size distribution, both for the total particles and for the BC particles specifically. Some of our analysis serves to support and extend previously determined relationships by considering a wider range of conditions, while other aspects are unique to this study. These observations provide a foundation for understanding and interpretation of experiments on the influence of photochemical aging on biomass particle properties, discussed in a related paper (Lim et al., 2019).

2 Methods

All experiments were conducted during the Fire Influence on Regional to Global Environments Experiment (FIREX) lab study, which took place at the Missoula Fire Sciences Lab in Missoula, MT, USA during November, 2016. Numerous types of biomass were combusted in a large chamber (12 x 12 x 19 m) and the smoke sampled to provide information on the physical, chemical, and optical properties of the resulting smoke (i.e., particulate and gas emissions). The general fuels types combusted included (exclusively or in combination): duff, dung, excelsior, straw, litter, untreated lumber, rotten debris, woody debris, shrub, herbaceous, and canopy biomass. A complete list of fuels and types is provided in Table S1, with further details available on the U.S. National Oceanic and Atmospheric Administration (NOAA) data archive

Formatted: Font: Bold

Deleted: Table S1

(https://esrl.noaa.gov/csd/projects/firex/). All data used in this publication are also available on the NOAA archive, with the processed data summarized in complementary data repository (Cappa et al., 2019a).

Both "room" and "stack" burns were conducted, although here we include results only from stack burns. During stack burns, the smoke was mixed with background room air and funneled up a large cylindrical stack (2 m dia. x 15 m height) where it was sampled into a high-flow transfer line at ca. 0.27 m^3/s. This flow rate corresponded to sampling approximately 10% of the stack flow. Smoke was transferred to an adjacent room via the high-flow transfer line (residence time ca. 2 s) where it was sub-sampled through a $PM_{2.5}$ cyclone and injected into a 0.25 m^3 Teflon photochemical reaction chamber (the mini chamber). Details on the construction and operation of the mini chamber can be found in (Lim et al., 2019). Here, we focus exclusively on the properties of particles sampled prior to initiation of photochemical oxidation; results of the photochemical oxidation experiments are discussed in a series of papers (Coggon et al., 2019;Lim et al., 2019). In brief, prior to each burn, the chamber was flushed with clean air with a relative humidity (RH) of approximately 40%. To fill the chamber, smoke was sub-sampled from the high-flow inlet and injected across the entire burn (typically lasting for 10-20 minutes) or until the chamber concentration reached a maximum. A suite of instruments sampled from the mini chamber at a flow rate of approximately 6 lpm. This flow rate varied from burn to burn due to the exact suite of instruments sampling. Clean makeup air was being injected simultaneously from a zero air generator to equal the air being sampled out of the chamber. The sampled smoke was diluted by a factor of ca. seven relative to the air in the high-flow inlet. Subsequent dilution after filling was characterized by the decay of acetonitrile (ACN). Properties of the primary particles are averaged over the 5-10 minute period after filling but before the initiation of photochemistry.

Particle-phase instrumentation sampled alternatingly every two minutes through a thermodenuded or ambient sample line. The thermodenuder was operated at 300 ºC with a residence time of approximately 5 s and volatilized semi-volatile components, including those that are internally mixed with BC. The ambient line was lined with a charcoal cloth that removed excess gases (such as VOCs, NO_x, and O_3) that could interfere with particle-phase measurements. Comparison of thermodenuded versus ambient particles allowed for the investigation of coating amount and volatility. The gas-phase composition in the mini chamber was similar to that sampled directly from the fire (Koss et al., 2018;Lim et al., 2019). Particle phase instrumentation included:

a multi-wavelength cavity-ringdown-photoacoustic absorption spectrometer (CRD-PAS) and a photoacoustic absorption spectrometer (PASS-3) for characterization of light absorption and extinction coefficients at 405 nm, 532 nm, and 781 nm; a high resolution aerosol mass spectrometer (HR-ToF-AMS) for characterization of non-refractory submicron particulate matter (NR-PM_1) components (i.e. OA, NO_3, SO_4, NH_4, Cl, K); a soot photometer AMS (SP-AMS) in laser-only mode for characterization of refractory BC and the NR-components that are internally mixed with BC; a single particle soot photometer (SP2) for characterization of refractory BC mass concentrations and size distributions; and a scanning electrical mobility sizer (SEMS) for measurement of particle mobility size distributions. Further details regarding instrument operation and calibration are provided in the Supplemental Material and in Lim et al. (2019).

3 Results and Discussion

3.1 Bulk optical property relationships

Due to the wide variety of biomass fuels and types used during FIREX, there was a substantial diversity in the properties of primary particles produced. Previous studies have shown both the single scatter albedo (SSA) and wavelength-dependence of absorption (the absorption Angstrom exponent, AAE) depend on the modified combustion efficiency (MCE) (Liu et al., 2013;McMeeking et al., 2014;Pokhrel et al., 2017). The MCE is defined here as:

$$\boldsymbol{MCE} = \frac{[\boldsymbol{CO_2}]}{[\boldsymbol{CO_2}]+[\boldsymbol{CO}]} \quad (1)$$

The SSA is defined as:

$$SSA = \frac{b_{ext}-b_{abs}}{b_{ext}} \quad (2)$$

where b_{ext} is the wavelength-specific extinction coefficient and b_{abs} is the wavelength-specific absorption coefficient. The AAE is defined as:

$$AAE = -\log(\frac{b_{abs,\lambda 1}}{b_{abs,\lambda 2}})/\log\left(\frac{\lambda 1}{\lambda 2}\right) \quad (3)$$

where λ_1 and λ_2 indicate two different wavelengths, here 405 nm and 532 nm. The MCE characterizes the overall combustion efficiency, with values closer to unity indicating more

complete combustion. In general, higher MCE correspond to more flaming combustion conditions while smaller MCE correspond to more smoldering conditions. We find a similar relationship between SSA_{405nm}, AAE, and [OA]/[BC] with MCE as previous studies (Figure 1) (McMeeking et al., 2009;Liu et al., 2013;McMeeking et al., 2014;Pokhrel et al., 2017). Specifically, the SSA_{405nm} is relatively constant and near unity for MCE < ~0.9, but above this value exhibits a rapid decline, albeit with a substantial amount of scatter (Figure 1a). The AAE is also relatively constant when MCE < 0.9, with very large values (AAE ~ 8). There is a rapid, scattered decrease in the AAE as MCE increases further (Figure 1b). The relationship between [OA]/[BC] and MCE is similar, with values generally decreasing as MCE increases but a large amount of scatter (Figure 1d). There is also a general relationship between the mass absorption coefficient referenced to BC (MAC_{BC}) at 405 nm and the MCE, but with similar scatter as the other properties (Figure 1c). The MAC_{BC} is defined as:

$$MAC_{BC} = b_{abs}/[BC] \quad (4)$$

The $MAC_{BC,405nm}$ includes contributions from absorption by BC, BrC, and from coating-induced enhancement of BC absorption. These results, along with the literature, indicate that MCE can provide guidance as to the general magnitude of these particle properties, but that the MCE is ultimately a fairly imprecise metric, especially for the SSA_{405nm}.

However, we find a very strong relationship between the SSA_{405nm} and the total [OA]/[BC] ratio (Figure 1e). This is consistent with the findings of Pokhrel et al. (2016), who observed something similar but over a smaller range of [OA]/[BC]. (Similarly strong relationships are observed for SSA values at 532 nm and 781 nm (Figure S1), or if the [NR-PM_1]/[BC] are used as OA averages 95% of the total NR-PM_1 mass.) Smaller [OA]/[BC] correspond to smaller SSA_{405nm} values with a sigmoidal relationship observed. (Fit parameters for all fits shown are provided in Table S1.) There is similarly a very strong, sigmoidal relationship between the AAE and $MAC_{BC,405nm}$ and [OA]/[BC] (Figure 1f,g). The large increase in the $MAC_{BC,405nm}$ indicates that BrC contributes substantially to the total absorption. The contributions of coating-induced enhancements and of BrC are discussed further in Sections 3.4.1 and 3.4.2. The larger range of [OA]/[BC] and the greater number of individual burns considered here, compared to Pokhrel et al. (2016), allows for determination of more robust fits. Pokhrel et al. (2017) found that the absorption

Deleted: Figure 1
Deleted: Figure 1
Deleted: Figure 1
Deleted: Figure 1
Deleted: Figure 1
Deleted: Figure 1
Deleted: Figure 1
Deleted: Figure S1
Formatted: Font: Bold
Deleted: Table S1
Deleted: Figure 1

enhancement at 405 nm, determined from thermodenuder measurements, increased with [OA]/[BC] up to [OA]/[BC] ~33 (the largest value reported), consistent with our findings.

These observations demonstrate that the optical properties of the primary particles depend on the relative amount of OA versus BC. This is as expected because OA is generally more scattering, compared to BC, and light absorbing OA (aka BrC) typically exhibits a much stronger wavelength dependence than BC. Based on these relationships, we divide the individual burns into different classes (Table 1). We have chosen to classify particles based on the observed SSA_{405nm} values; use of [OA]/[BC] for classification yields largely similar results, given the strong relationship between the two. The dividing lines between classes are selected to yield six classes that span the entire range of SSA_{405nm} values, from 0.23 (Class 1) to 0.97 (Class 6), with approximately equal numbers of individual burns in each class (ca. 8-10). Partitioning the observations into different particle classes facilitates interpretation of the photochemical evolution of the particles, to be discussed in future work. In addition, we find that use of the Class average properties versus MCE generally provides more representative fits to the observations (visually apparent in Figure 1, and supported by the reduced χ^2 for the fits).

Formatted: Font: Bold

Deleted: Table 1

Deleted: Figure 1

3.2 OA composition and volatility

Variability in the bulk composition of the OA is characterized by the O:C and H:C atomic ratios and the fractional abundance (f_x) of two marker ions, m/z = 44 and m/z = 60. The f_{44} is complementary to O:C and larger values generally indicate a greater degree of oxygenation and the presence of carboxylic acids. The f_{60} is often taken as a marker ion for biomass burning, in particular a signature of levoglucosan and similar molecules (Schneider et al., 2006;Alfarra et al., 2007). The high resolution ion $C_2H_4O_2^+$ contributes to and exhibits similar behavior as f_{60}; the slope for $f_{C2H4O2+}$ against f_{60} is 0.98. While it is known that properties such as f_{60} vary in different biomass burning samples (Schneider et al., 2006) or between near-source intercepts of different ambient plumes (Garofalo et al., 2019), the specific dependence on burn conditions or overall particle composition (e.g. [OA]/[BC]) has not been systematically explored to our knowledge.

The average f_{60} = 0.022 ± 0.01 (1σ). The f_{60} values vary non-monotonically with [OA]/[BC], exhibiting a slight increase from Class 1 to Class 3 and then a decrease from Class 4 to Class 6 (Figure 2a). This indicates that, while f_{60} is overall a useful marker ion for biomass burning, it

cannot be used to distinguish between different burn conditions. The f_{44} generally decreases with [OA]/[BC] (Figure 2b; r^2 = 0.33.) However, the average f_{44} values for particle Classes 2-5 differ negligibly, suggesting that f_{44} might be useful in discriminating between extreme cases (e.g. Class 1 versus Class 6), but that it is of limited general use in distinguishing between burn conditions and fuel types. The O:C atomic ratio (average = 0.37 ± 0.09) exhibits similar behavior—expected as f_{44} is generally related to O:C (Aiken et al., 2008)—with a general decrease as [OA]/[BC] increases, although a comparably weaker correlation (Figure 2c; r^2 = 0.17). The H:C (average = 1.76 ± 0.05) exhibits a weak, positive correlation with [OA]/[BC], although the variability is slight (Figure 2d; r^2 = 0.27).

The mass fraction of the OA that is composed of nitrated organics ($f_{ON\text{-}OA}$ = [ON]/[OA]) was determined using the HR-ToF-AMS measurements and the method of Kiendler-Scharr et al. (2016) (see the Supplemental Material for further details). The terminology nitrated organics (ON) includes contributions from both nitro and nitrate functional groups. The fraction of measured nitrate that was ON ($f_{ON\text{-}N}$ = [ON]/([ON]+[NO_3^-])) decreased with [OA]/[BC] and ranged from 0.91 (Class 1) to 0.48 (Class 6) (**Figure S2a**). The Class-specific average $f_{ON\text{-}OA}$ also decreased with [OA]/[BC], although by a much greater extent than the $f_{ON\text{-}N}$, ranging from 6.0% (Class 1) to 0.27% (Class 6) and (**Figure 2e**). There is a reasonably linear relationship between log($f_{ON\text{-}OA}$) and log([OA]/[BC]) (r^2 = 0.47). This indicates that a larger proportion of ON species and functionalities are produced when particles are, on average, more BC-rich. This does not reflect differences in fuel nitrogen content as there is no relationship between fuel N and $f_{ON\text{-}OA}$ (**Figure S2b**). Therefore, it seems that the relationship between $f_{ON\text{-}OA}$ and [OA]/[BC] is related more so to the burn conditions than the fuel N content, although as with many other properties the relationship with [OA]/[BC] is clearer than with the MCE (**Figure S2c**).

The OA volatility is characterized as the ratio between the OA concentration after thermodenuding to that without thermodenuding (the mass fraction remaining, MFR_{OA}). The MFR_{OA} decreases as [OA]/[BC] increases (**Figure 2f**), indicating that the OA at lower [OA]/[BC] is less volatile than the OA at higher values. This observation provides support for the proposal by Saleh et al. (2014) that less volatile, more absorbing species are preferentially formed under conditions where BC formation is favored, discussed further in Section 3.4.2. The relationship between MFR_{OA} and [OA]/[BC] is reasonably described by an exponential function.

Formatted: Font: Bold
Deleted: Figure S2
Deleted: Figure 2
Formatted: Font: Bold
Formatted: Font: Bold
Deleted: Figure S2
Deleted: Figure S2
Formatted: Font: Bold
Formatted: Font: Bold
Deleted: Figure 2

3.3 BC Mixing State

As discussed above, the relative amounts of OA and BC vary greatly between fuel types and combustion conditions. However, the distribution of BC and OA between particles, and how this varies between very different burn conditions, has not been previously explored in detail to our knowledge. The bulk average fraction of OA that is internally mixed with BC versus OA that is externally mixed from BC is determined using the HR-ToF-AMS and SP-AMS measurements. The HR-ToF-AMS quantifies OA independent of mixing state, whereas the SP-AMS (as operated here) quantifies only the OA that is internally mixed with BC. The fraction of OA that is internally mixed with BC ($f_{OA,int}$) is:

$$f_{OA,int} = \frac{[OA]_{SP-AMS}}{[OA]_{HR-ToF-AMS}} = \frac{[OA]_{int}}{[OA]_{tot}} \quad (5)$$

where the subscript *int* indicates the OA that is internally mixed with BC and the subscript *tot* indicates the total OA. The $f_{OA,int}$ should range from 0 to 1. Related, the SP-AMS quantified the ratio between the OA that is internally mixed with BC and the BC concentration, referred to here as $[OA]_{int}/[BC]$. We find that $f_{OA,int}$ decreases substantially as [OA]/[BC] increases, ranging from $f_{OA,int} = 0.4$ for Class 1 (low SSA) particles to $f_{OA,int} = 0.01$ for Class 6 (high SSA) particles (**Figure 3a**). The data are well-fit by a sigmoidal function. However, the amount of OA coating BC ($R_{OA\text{-}BC} = [OA]_{int}/[BC]$) increases with the total [OA]/[BC], also with a sigmoidal relationship (**Figure 3b**). Thus, while a smaller fraction of the total OA is internally mixed with BC for larger total [OA]/[BC] the amount of OA that coats BC increases. Most likely this behavior reflects that BC and OA are generated with different efficiencies in different parts of the combusting biomass. BC is more efficiently generated from flaming combustion while OA is more efficiently generated from smoldering combustion. These observations demonstrate that the extent to which atmospheric models can assume that all OA is internally mixed with or externally mixed from BC at the point of emission will depend on the combustion conditions.

Deleted: Figure 3

Deleted: Figure 3

3.4 Absorption enhancement and brown carbon

3.4.1 Coating-induced absorption enhancement

Non- or weakly-absorbing coatings on black carbon particles can theoretically increase the absorption by BC (Fuller et al., 1999;Bond et al., 2006), an effect which has been confirmed by

laboratory experiments (Lack et al., 2009;Shiraiwa et al., 2010;Cappa et al., 2012). The extent to which coatings on BC actually enhance absorption by BC in the atmosphere remains unclear. Some studies indicate minor coating-induced enhancements while others indicate substantial enhancements (Cappa et al., 2012;Healy et al., 2015;Liu et al., 2015;Peng et al., 2016;Zhang et al., 2016;Liu et al., 2017;Cappa et al., 2019b). Understanding the nature of the coating-induced enhancement is important for quantifying the radiative impacts of BC (Jacobson, 2001;Bond et al., 2013). Further, these coating-induced absorption enhancements ($E_{abs.coat}$) complicate the determination of brown carbon (BrC) absorption and the two must be separated. Here, we examine the extent to which coatings on BC for primary biomass burning particles enhance the BC absorption. Theoretically, the magnitude of $E_{abs,coat}$ for an individual particle depends primarily on the coating thickness and secondarily on the size of the BC core (Bond et al., 2006; Fuller et al., 1999). Thus, the extent to which coatings enhance BC absorption for a given situation can be assessed through the relationship between the observed MAC_{BC} and the coating-to-core mass ratio ($R_{coat\text{-}rBC}$ = $[NR\text{-}PM]_{int}/[BC]$, where *int* indicates that the coating material is internally mixed with BC). The expectation is that the MAC_{BC} increases with $R_{coat\text{-}BC}$.

However, absorption by BrC can also lead to an apparent increase in the normalized absorption with R_{BC} if the BrC abundance correlates with the total coating amount. Because BrC absorbs more strongly at shorter wavelengths, the wavelength-dependence of the MAC_{BC} to R_{BC} relationship can be used to further separate the influence of coating versus BrC absorption. The MAC_{BC} exhibits a wavelength-dependent relationship with $R_{coat\text{-}rBC}$ for fresh biomass particles (405 nm, 532 nm and 781 nm) (**Figure 4a-c**). The MAC_{BC} increases notably with $R_{coat\text{-}rBC}$ at 405 nm and to a lesser extent at 532 nm. At 781 nm the MAC_{BC} is essentially independent of $R_{coat\text{-}rBC}$ up to $R_{coat\text{-}rBC}$ values as large as 10, but does exhibit some increase at $R_{coat\text{-}rBC} > 10$. However, this is most likely a result of absorption by OA at 781 nm and not indicative of an increase in the coating-induced enhancement, discussed further below. The wavelength dependence provides clear evidence of BrC absorption at shorter wavelengths.

Deleted: Figure 4

That the MAC_{BC} at 781 nm is nearly independent of $R_{coat\text{-}rBC}$ up to such large $R_{coat\text{-}rBC}$ values indicates that there is only a minor coating-induced enhancement for the primary biomass particles, the magnitude of which is discussed below. Our observations are consistent with McMeeking et al. (2014), who also investigated the relationship between the MAC_{BC} and $R_{coat\text{-}rBC}$ for a primary biomass particles from multiple fuel types. Most likely, this lack of a substantial coating-induced

enhancement results from a non-even distribution of non-BC mass across the population of BC particles (Fierce et al., 2016;Liu et al., 2017) and from the morphology of BC-containing particles not conforming to an idealized core-shell structure (Adachi et al., 2010). The influence of photochemical aging on the coating-induced enhancement will be examined in future work.

The relationship between MAC_{BC} and the coating amount ($R_{coat\text{-}rBC}$) can be contrasted with the relationship between MAC_{BC} and the total [OA]/[BC]. At all three wavelengths the MAC_{BC} exhibit strong, sigmoidal relationships with [OA]/[BC] (**Figure 4d-f**). That $MAC_{BC,781nm}$ exhibits such a clear relationship with [OA]/[BC] suggests that even the small apparent coating-induced enhancement, implied above from the very weak with $R_{coat\text{-}rBC}$, is largely driven by absorption by BrC rather than from the impact of coating on BC. Pokhrel et al. (2017) found that the absorption enhancement, determined from thermodenuder measurements, increased notably with [OA]/[BC] up to [OA]/[BC] ~33 at 405 nm (the largest value reported by them), but by much less at 660 nm, consistent with our findings.

The observations allow for determination of wavelength-dependent MAC_{BC} values for pure BC ($MAC_{BC,pure}$) for each wavelength by extrapolation of the MAC_{BC} versus [OA]/[BC] ratio to zero using sigmoid fits. Since the $R_{coat\text{-}rBC}$ correlates reasonably with [OA]/[BC] (**Figure 3b**), extrapolation against [OA]/[BC] to zero effectively removes both contributions from BrC and any coating-induced enhancement. The derived $MAC_{BC,pure}$ values are 11.8 $m^2\ g^{-1}$ at 405 nm, 8.8 $m^2\ g^{-1}$ at 532 nm and 5.5 $m^2\ g^{-1}$ at 781 nm, with estimated fit-based uncertainties of ~10%. The absolute uncertainties on the $MAC_{BC,pure}$ are primarily dependent on the uncertainty in the b_{abs} and [rBC] measurements, and are ~35%. The derived MAC_{BC} values are very similar to those recently reported by Forestieri et al. (2018) for fresh BC particles: $MAC_{BC,pure}$ = 11.9 $m^2\ g^{-1}$ at 405 nm and 8.8 $m^2\ g^{-1}$ at 532 nm, with an extrapolated value at 781 nm of 5.7 $m^2\ g^{-1}$. The value at 532 nm is somewhat higher than that suggested by Bond and Bergstrom (2006) (7.75 $m^2\ g^{-1}$ at 532 nm). Our derived $MAC_{BC,pure}$ values yield an AAE = 1.17, determined from a fit to the three wavelengths. An AAE close to unity indicates absorption is dominated by BC, as expected.

Values for the absorption enhancement at 781 nm are calculated as the ratio between the observed MAC_{BC} in **Figure 4** and the derived $MAC_{BC,pure}$. The derived E_{abs} range from 0.96 to 27. Values greater than two occur only for the particles having particularly large [OA]/[BC], > 400. As E_{abs} values much greater than two at 781 nm are unlikely to result from mixing-induced

Deleted: Figure 4

Deleted: Figure 3

Deleted: Figure 4

enhancements (Chakrabarty and Heinson, 2018), this again suggests that the OA is somewhat absorbing at this wavelength. For the burns where [OA]/[BC] < 400, the median E_{abs} = 1.14 and the arithmetic mean E_{abs} = 1.19 ± 0.14 (1σ). Given that some of this enhancement may result from BrC absorption at 781, these values can be considered upper-limits on $E_{abs,coat}$, and the small magnitude is consistent with our conclusion above that, while likely greater than zero, the mixing-induced enhancement is generally minor. It is possible that the $E_{abs,coat}$ values when [OA]/[BC] > 400 are substantially larger. However, given the general lack of a dependence of the $MAC_{BC,781nm}$ for $R_{BC\text{-}coat}$ < 10 this seems unlikely.

Deleted: negligible

3.4.2 Primary brown carbon absorption

The absorption due to brown carbon is determined by difference as:

$$\boldsymbol{b_{abs,BrC} = b_{abs,obs} - MAC_{BC,pure} \cdot [BC] \cdot E_{abs,coat}} \quad \textbf{(6)}$$

where $b_{abs,BrC}$ is the absorption due to BrC specifically. Importantly, the use of study-specific $MAC_{BC,pure}$ values serves to reduce systematic biases in the $b_{abs,BrC}$, compared to direct use of literature $MAC_{BC,pure}$ values. Assuming $E_{abs,coat}$ = 1 provides an upper limit on the BrC absorption, which we note is likely most appropriate for the particles sampled here, as discussed in the previous section. Therefore, we use the upper-limit values throughout the analysis that follows, unless otherwise stated. However, a lower limit for BrC absorption can be determined at 405 nm and 532 nm assuming that all of the enhancement at 781 nm results from coatings and not from BrC. The resulting $E_{abs,obs}$ (= $MAC_{BC,obs}/MAC_{BC,pure}$) at 781 nm averages 1.19 for $R_{BC\text{-}coat}$ < 10. Using $E_{abs,coat}$ = 1.19 in Eqn. 7 yields a lower limit for the BrC absorption at the two shorter wavelengths, appropriate since $E_{abs,coat}$ generally has only a small wavelength dependence. A fit to the coating-corrected (lower-limit) versus upper-limit $b_{abs,BrC}$ yields a slope of 0.97 at 405 nm and 0.88 at 532 nm (**Figure S3**). The smaller difference at 405 nm results from the fractional contribution of BrC to the total absorption being larger at this wavelength.

Deleted: Figure S3

Brown carbon-specific mass absorption coefficients (MAC_{BrC}) are determined as the ratio between $b_{abs,BrC}$ and the total OA concentration:

$$\boldsymbol{MAC_{BrC} = \frac{b_{abs,BrC}}{[OA]}} \quad (7)$$

The MAC_{BrC} values from Eqn. **7** are bulk-average values, and do not account for different molecules and classes of molecules likely having different absorptivities. Uncertainties in the MAC_{BrC} values are determined by error propagation. Similarly, an AAE value for just the brown carbon (AAE_{BrC}) can be calculated using wavelength pairs as:

$$\boldsymbol{AAE_{BrC}} = -\log\left(\frac{b_{abs,BrC,\lambda_1}}{b_{abs,BrC,\lambda_2}}\right) / \log\left(\frac{\lambda_1}{\lambda_2}\right); \quad (8)$$

The geometric averages of the MAC_{BrC} values are $0.76^{+0.65}_{-0.35}$ m^2 g^{-1}, $0.21^{+0.36}_{-0.13}$ m^2 g^{-1}, $0.056^{+0.15}_{-0.04}$ m^2 g^{-1} at 405 nm, 532 nm and 781 nm, with uncertainties the 1σ burn-to-burn variability. The MAC_{BrC} values vary between classes, generally increasing as the [OA]/[BC] ratio decreases at all wavelengths (shown for 405 nm in Figure 5a). For example, the average MAC_{405nm} = 2.3 ± 1 m^2 g^{-1} for Class 1 and 0.35 ± 0.09 m^2 g^{-1} for Class 6. Although the uncertainties on the derived MAC_{BrC} increase substantially as [OA]/[BC] decreases—because BrC absorption contributes to a smaller extent at longer wavelengths—the observations nonetheless indicate that the BrC absorptivity depends on the combustion conditions. The relationship at 405 nm is well-described by a sigmoidal function in log-log space, with limiting values of 0.35 m^2 g^{-1} at large [OA]/[BC] and 11.2 m^2 g^{-1} at small [OA]/[BC]. That the extrapolated zero [OA]/[BC] limit for MAC_{BrC} is similar to pure BC suggests an evolution of BrC towards having properties similar to BC when the overall [OA] content is small. Such behavior is consistent with Saleh et al. (2018), who argue that there is a continuum of BrC properties that depends on the combustion conditions, as demonstrated in that study for low-temperature benzene and toluene combustion. The range of the MAC_{BrC} values observed here, including that there is notable absorption at 781 nm, encompass many previous measurements, summarized in Table S3. This likely reflects the wide diversity of fuel types and burn conditions considered here, as exemplified by the very large range of [OA]/[BC].

Estimated values of the imaginary component of the refractive index for BrC (k_{BrC}) are determined from Mie theory via optical closure (Zhang et al., 2016), assuming a real part of the refractive index of 1.5 and a particle diameter of 150 nm, a typical value for these experiments. Imaginary RI values are of use in atmospheric models for calculation of BrC absorption. There is a linear relationship between MAC_{BrC} and k_{BrC} (Figure S4a). Thus, the k_{BrC} exhibits a similar correlation with [OA]/[BC] as does the MAC_{BrC} (Figure 5a).

Deleted: Figure 5

Formatted: Font: Bold

Deleted: Table S3

Deleted: Figure S4

Deleted: Figure 5

The wavelength-dependence of absorption, i.e. the $AAE_{405\text{-}532}$, also varies with [OA]/[BC], in this case with a positive relationship between the two (Figure 5b). The relationship is reasonably described by a sigmoidal function. This implies that, while the MAC_{BrC} varies inversely with [OA]/[BC] at all wavelengths, the exact variation is wavelength dependent. The $AAE_{405\text{-}532}$ relationship with [OA]/[BC] is well-described by a sigmoidal function (versus log([OA]/[BC]), with limiting values of 10.4 at large [OA]/[BC] and 1.3 at small [OA]/[BC]. The wavelength-dependence of the k_{BrC} (w_{BrC}) are also calculated, to facilitate comparison with the literature, as:

$$w_{BrC} = -\log\left(\frac{k_{BrC,\lambda1}}{k_{BrC,\lambda2}}\right)/\log\left(\frac{\lambda1}{\lambda2}\right) \quad (9)$$

The w_{BrC} exhibit a similar dependence on [OA]/[BC] as the AAE_{BrC}, as the w_{BrC} and AAE_{BrC} are linearly related, albeit with some scatter (Figure S4b; $r^2 = 0.97$).

Our observations support the results of Saleh et al. (2014), who also found a relationship between the $k_{BrC,405nm}$ and [OA]/[BC]. However, our analysis substantially extends the range of [OA]/[BC] values investigated in that work (they considered [OA]/[BC] from only ca. 2 to 170). In the overlap region between our two studies the $k_{BrC,405nm}$ agree reasonably well over the range 2 < [OA]/[BC] < 50, but the $k_{BrC,405nm}$ from Saleh et al. (2014) are smaller than observed here above [OA]/[BC] = 50. Importantly, our results demonstrate that the linear fit suggested by Saleh et al. (2014) for MAC_{BrC} is only appropriate over the range of values they considered and that a sigmoidal provides for a more robust relationship over a wider range of [OA]/[BC]. Related, the wider range of [OA]/[BC] enables more robust determination of the functional dependence of the wavelength-dependence of absorption (w_{BrC}), with overall larger w_{BrC} values and a larger plateau at high [OA]/[BC] compared to the fit by Saleh et al. (2014).

The MAC_{BrC} values also correlate with the nitrated organic fraction of OA, the latter of which, as noted above, also correlates with the [OA]/[BC] (Figure 6a). This observation suggests that organic nitrate and nitro functionalities may be at least somewhat responsible for the increase in absorption. Laskin et al. (2018) performed offline molecular level analyses of primary OA collected during FIREX. They found that nitroaromatics and N-containing polycyclic aromatic hydrocarbons (PAHs) contribute notably to the total light absorption by BrC, although there are many non-N-containing species that also contribute to BrC absorption. The variability between particle Classes is consistent with the results of Lin et al. (2016), which show that the abundance

Deleted: Figure 5

Deleted: Figure S4

Deleted: Figure 6

of N-containing chromophores varies between particles produced from different biomass fuels. Additionally Mohr et al. (2013) observed a relationship between the concentration of nitrated phenols and short-wavelength absorption by BrC, although it is possible that for their measurements these species were produced from chemical processing, as opposed to being directly emitted. Altogether, our results provide support for the idea that nitrated organic functionalities are an important contributor to BrC absorption. However, it is very likely that other functional groups also contribute to the total absorption.

The $MAC_{BrC,405nm}$ exhibits an inverse correlation with the f_{60}/f_{44} ratio of the OA, although there is substantial scatter in the f_{60}/f_{44} ratio for a given particle class (Figure 6b). (The f_{44} and f_{60} have no discernable relationship.) The observed $MAC_{BrC,405nm}$ relationship with f_{60}/f_{44} is opposite that reported by Lack et al. (2013) for ambient measurements of particles a biomass burning plume, who find a reasonable positive correlation. This difference in behavior results from our sampling primary particles directly—thereby focusing on the inherent variability in the properties of the emitted particles—while Lack et al. (2013) sampled ambient particles. For ambient sampling, the observed relationship will be sensitive to mixing of biomass burning particles with background or aged biomass particles, which are known to have a smaller f_{60} (Cubison et al., 2011). Thus, the relationship observed by Lack et al. (2013) can best be viewed as a mixing line between the fresh primary particles (having large $MAC_{BrC,405nm}$ and large f_{60}/f_{44}) and background or aged biomass particles (having small $MAC_{BrC,405nm}$ and small f_{60}/f_{44}), rather than providing information on the inherent variability in the absorptivity of the fresh particles.

Deleted: Figure 6

3.5 Size distributions

Total particle mobility size distributions and BC-only size distributions were measured (Figure 7). Primary particle size distributions are important parameters specified in regional and global models. The number-weighted and volume-weighted size distributionare generally described by either one or two log-normal modes for individual burns; a two-mode fit provides a more robust solution across all modes. The mass-weighted BC size distributions are similarly described by one or two log-normal modes. A fit to the average number-weighted distribution across all particle classes yields geometric median diameters ($d_{p,N}$) and widths (σ_g) of 60.3 nm and 1.76, respectively, for the smaller mode and 153 nm and 1.64 for the larger mode (Figure 8). The amplitude of the smaller mode is 4.6 times the larger mode. A single mode fit yields $d_{p,N}$ = 68 nm and χ_g = 1.93,

Deleted: Figure 7

Deleted: Figure 8

476 although the fit is poorer. Mann et al. (2014) report $d_{p,N}$ values used by a variety of global models
477 for biofuels. The models tend to use either 80 nm or 150 nm, although a few use other values (30
478 nm, 60 nm, 100 nm). Those using 80 nm typically use $\sigma_g = 1.80$ while those using 150 nm typically
479 use $\sigma_g = 1.59$, although there are exceptions. Our observations indicate that use of a bimodal
480 distribution within models would be more representative, but that a single mode can do acceptably.
481 We find that the volume-weighted distribution calculated from a single-mode fit to the number-
482 weighted distribution is similar to the observed volume-weighted distribution (Figure 8). Thus,
483 the use of a single-mode to represent biomass burning size distributions thus appears acceptable,
484 so long as the appropriate parameters are used. In this context, the widths of the distribution used
485 by the various global models appear somewhat too small. However, we note that the microphysics
486 occurring in the fresh smoke sampled here, which will govern the size distributions, may differ
487 from that in atmospheric plumes.

Deleted: Figure 8

488 The average BC-specific mass-weighted size distribution mode is at 148 nm (Figure 8). A
489 bimodal fit yields values for the mass median diameter ($d_{p,M}$) and σ_g of 137.2 nm and 1.62,
490 respectively, for the smaller mode and 197.1 nm and 1.24 for the larger mode, with most of the
491 mass contained in the smaller mode. May et al. (2014) report $d_{p,M}$ from laboratory biomass
492 combustion ranging from 140-190 nm, averaging 170 nm. Their average is somewhat larger than
493 ours, likely reflecting differences in the exact fuels sampled. The mode diameter for the BC-
494 specific distribution is especially smaller than observed for biomass burning particles from some
495 ambient observations, which tend to give values closer to 200 nm (Schwarz et al., 2008;Kondo et
496 al., 2011;Sahu et al., 2012;May et al., 2014;Cappa et al., 2019b). This difference between lab and
497 field observations was also noted by May et al. (2014). We speculate that the influence of
498 coagulation may be suppressed in our experiments relative to what occurs in the atmosphere due
499 to slower overall dilution, leading to smaller BC size distributions. To the extent this is the reason
500 for the difference, the total particle distributions would also be biased towards too small particles,
501 compared to the atmosphere. However, there is no relationship between $d_{p,N}$ and the total particle
502 number concentration for our experiments. Formation of secondary aerosol in the near-field of a
503 sampled ambient plume could also contribute to this difference.

Deleted: Figure 8

504 There is substantial variability between individual burns within a given particle Class in terms
505 of the shape of the size distributions (Figure 7). This variability is most evident for Class 1, 2 and

Deleted: Figure 7

5, but present for all Classes. Nonetheless, the number-weighted mean diameter ($d_{p,N,mean}$) appears to decrease somewhat with MCE (Figure 9; $r^2 = 0.38$). However, the relationship is largely driven by the Class 6 particles, which generally have lower MCE values, having larger $d_{p,N,mean}$ values. A lack of any particularly clear relationship is consistent with Hosseini et al. (2010), who observed the $d_{p,N,mean}$ to exhibit a complex relationship with combustion conditions. The $d_{p,N,mean}$ varies non-monotonically with [OA]/[BC], with particle size first decreasing slightly as [OA]/[BC] increases (from Class 1 to Class 3) and then increasing with further increases in [OA]/[BC] (from Class 4 to Class 6) (Figure 9). This is despite the notable burn-to-burn variability. It is important to note that the mobility-based size is particle shape-dependent; very BC-rich particles are more likely to have non-spherical shapes and thus have larger mobility diameters. This could explain the minimum in $d_{p,N}$ around Class 3 particles, for which [OA]/[BC] = 10.

Some of the variability within a class appears related to the presence of different fuel types within a class. Number-weighted and BC-specific mass-weighted size distributions by fuel type are shown in Figure 10. For the number-weighted distributions, leaf litter and rotten logs exhibit the greatest variability between different burns, although we note that multiple burns were not performed for all fuels. The shapes of the leaf litter, peat and "other" fuel types differ most notably from the other fuel types, with the presence of more than one mode more apparent. (The "other" category here includes non-traditional biofuels, specifically building materials and excelsior.) For the BC-specific size distributions, the litter, canopy, and duff exhibited the greatest intra-fuel variability. For most fuels, the BC-specific distribution peaks around 150 nm, as noted above. However, for a subset of burns (eight of them) the BC-specific distribution peaks around 100 nm (Figure 10). These small BC-mode distributions occur for the OA-rich particle classes 4, 5 and 6 (Figure 7), although there is no clear pattern to their occurrence.

Deleted: Figure 9

Deleted: Figure 9

Deleted: Figure 10

Deleted: Figure 10

Deleted: Figure 7

4 Conclusions and Implications

Measurements of primary particles produced from combustion of a variety of biomass fuel types indicate the optical, physical, and chemical properties of the emitted particles exhibit wide variability. We show that variability in many optical properties (e.g. single scatter albedo, wavelength dependence of absorption, mass absorptivity of black and brown carbon) is directly linked to the [OA]/[BC] ratio of the emitted particles; the relationships with [OA]/[BC] are much stronger than with the commonly used modified combustion efficiency, and mathematical

relationships between the various properties are determined. However, the absorption enhancement due to coating of BC (the so-called "lensing" effect) is shown to be minor and essentially independent of the amount of coating up to large coating-to-BC mass ratios. The brown carbon mass absorptivity correlates with the nitrated organic fraction of OA, suggesting that nitrated organic species contribute to BrC absorption. Many bulk chemical properties (i.e. O:C, H:C, and the relative concentrations of key marker ions such as f_{60}) exhibit limited dependence on the burn conditions and the [OA]/[BC] ratio. However, both the OA volatility and nitrated organic fraction of OA decrease with [OA]/[BC]. The fraction of OA that is internally mixed with BC was shown to decrease strongly with the [OA]/[BC] ratio, from nearly all OA being internally mixed with BC when the particles are overall BC-rich to only a few percent of OA being mixed with BC when OA dominates. Yet, the relative amount of OA coating the BC increases with [OA]/[BC]; that is, when more of the OA is externally mixed from BC those particles that do contain BC nonetheless have thicker OA coatings. The observed total particle size distributions are reasonably well described by a single log-normal mode, but are better fit using a bimodal distribution. The BC-specific size distributions are similarly best fit using a bimodal distribution, although a single mode provides a reasonable representation. The dependence of the geometric median mobility diameter on the burn conditions or particle state (i.e. the [OA]/[BC]) is complicated by the mobility diameter being sensitive to variations in particle shape, which depend on the [OA]/[BC] ratio. Overall, these results expand on previous observations of primary biomass burning particle properties, considering a wider range of [OA]/[BC] and associated properties. Further, they provide a foundation for understanding the post-emission evolution of biomass burning smoke due to photochemical oxidation as discussed in Lim et al. (2019).

Deleted: negligible

5 Data Availability

All data are available from the NOAA FIREX-AQ data repository (https://esrl.noaa.gov/csd/projects/firex/firelab/). This includes a summary of the fuel types used for each burn and the measurement time-series for each burn. The primary particle averages used in this work are additionally collected in the UC DASH data repository (Cappa et al., 2019a).

6 Author Contributions

CDC and JHK designed the experiments. CDC, CYL, and DHH carried out the measurements and data processing. CDC, CDM, and CYL analyzed data. CDC and CDM wrote the manuscript, with contributions from all co-authors.

7 Acknowledgements

This work was supported by the National Oceanic and Atmospheric Administration Atmospheric Chemistry, Carbon Cycle & Climate Program, awards NA16OAR4310111 and NA16OAR4310112. CYL was additionally supported by the National Science Foundation Graduate Research Fellowship Program. The entire FIREX team, especially Bob Yokelson and Jim Roberts and the staff of the Missoula Fire Sciences Laboratory, are acknowledged for their assistance. Putting together the community inlet was a community effort—thank you to all who contributed. Shuka Schwarz and Gavin McMeeking are also thanked for their assistance with the SP2.

8 References

Adachi, K., Chung, S. H., and Buseck, P. R.: Shapes of soot aerosol particles and implications for their effects on climate, J. Geophys. Res., 115, D15206, https://doi.org/10.1029/2009jd012868, 2010.

Adler, G., Flores, J. M., Abo Riziq, A., Borrmann, S., and Rudich, Y.: Chemical, physical, and optical evolution of biomass burning aerosols: a case study, Atmos. Chem. Phys., 11, 1491-1503, https://doi.org/10.5194/acp-11-1491-2011, 2011.

Aiken, A. C., Decarlo, P. F., Kroll, J. H., Worsnop, D. R., Huffman, J. A., Docherty, K. S., Ulbrich, I. M., Mohr, C., Kimmel, J. R., Sueper, D., Sun, Y., Zhang, Q., Trimborn, A., Northway, M., Ziemann, P. J., Canagaratna, M. R., Onasch, T. B., Alfarra, M. R., Prevot, A. S. H., Dommen, J., Duplissy, J., Metzger, A., Baltensperger, U., and Jimenez, J. L.: O/C and OM/OC ratios of primary, secondary, and ambient organic aerosols with high-resolution time-of-flight aerosol mass spectrometry, Environ. Sci. Technol., 42, 4478-4485, https://doi.org/10.1021/es703009q, 2008.

Alexander, D. T. L., Crozier, P. A., and Anderson, J. R.: Brown Carbon Spheres in East Asian Outflow and Their Optical Properties, Science, 321, 833-836, https://doi.org/10.1126/science.1155296, 2008.

Alfarra, M. R., Prevot, A. S. H., Szidat, S., Sandradewi, J., Weimer, S., Lanz, V. A., Schreiber, D., Mohr, M., and Baltensperger, U.: Identification of the Mass Spectral Signature of Organic Aerosols from Wood Burning Emissions, Environmental Science & Technology, 41, 5770-5777, https://doi.org/10.1021/es062289b, 2007.

Andreae, M. O., and Merlet, P.: Emission of trace gases and aerosols from biomass burning, Global Biogeochemical Cycles, 15, 955-966, https://doi.org/doi:10.1029/2000GB001382, 2001.

Bluvshtein, N., Lin, P., Flores, J. M., Segev, L., Mazar, Y., Tas, E., Snider, G., Weagle, C., Brown, S. S., Laskin, A., and Rudich, Y.: Broadband optical properties of biomass-burning aerosol and identification of brown carbon chromophores, Journal of Geophysical Research: Atmospheres, 122, 5441-5456, https://doi.org/doi:10.1002/2016JD026230, 2017.

Bond, T. C., and Bergstrom, R. W.: Light absorption by carbonaceous particles: An investigative review, Aerosol Science and Technology, 40, 27-67, https://doi.org/10.1080/02786820500421521, 2006.

Bond, T. C., Habib, G., and Bergstrom, R. W.: Limitations in the enhancement of visible light absorption due to mixing state, J. Geophys. Res.-Atmos., 111, https://doi.org/10.1029/2006JD007315, 2006.

Bond, T. C., Doherty, S. J., Fahey, D. W., Forster, P. M., Berntsen, T., DeAngelo, B. J., Flanner, M. G., Ghan, S., Kärcher, B., Koch, D., Kinne, S., Kondo, Y., Quinn, P. K., Sarofim, M. C., Schultz, M. G., Schulz, M., Venkataraman, C., Zhang, H., Zhang, S., Bellouin, N., Guttikunda, S. K., Hopke, P. K., Jacobson, M. Z., Kaiser, J. W., Klimont, Z., Lohmann, U., Schwarz, J. P., Shindell, D., Storelvmo, T., Warren, S. G., and Zender, C. S.: Bounding the role of black carbon in the climate system: A scientific assessment, Journal of Geophysical Research: Atmospheres, 118, 1-173, https://doi.org/10.1002/jgrd.50171, 2013.

Bruns, E. A., Perraud, V., Zelenyuk, A., Ezell, M. J., Johnson, S. N., Yu, Y., Imre, D., Finlayson-Pitts, B. J., and Alexander, M. L.: Comparison of FTIR and Particle Mass Spectrometry for the

626 Measurement of Particulate Organic Nitrates, Environmental Science & Technology, 44, 1056-
627 1061, https://doi.org/10.1021/es9029864, 2010.

628 Canagaratna, M. R., Jayne, J. T., Jimenez, J. L., Allan, J. D., Alfarra, M. R., Zhang, Q., Onasch,
629 T. B., Drewnick, F., Coe, H., Middlebrook, A., Delia, A., Williams, L. R., Trimborn, A. M.,
630 Northway, M. J., DeCarlo, P. F., Kolb, C. E., Davidovits, P., and Worsnop, D. R.: Chemical and
631 microphysical characterization of ambient aerosols with the Aerodyne aerosol mass spectrometer,
632 Mass Spectrometry Reviews, 26, 185-222, https://doi.org/10.1002/mas.20115, 2007.

633 Cappa, C. D., Onasch, T. B., Massoli, P., Worsnop, D., Bates, T. S., Cross, E., Davidovits, P.,
634 Hakala, J., Hayden, K., Jobson, B. T., Kolesar, K. R., Lack, D. A., Lerner, B., Li, S. M., Mellon,
635 D., Nuaanman, I., Olfert, J., Petaja, T., Quinn, P. K., Song, C., Subramanian, R., Williams, E. J.,
636 and Zaveri, R. A.: Radiative absorption enhancements due to the mixing state of atmospheric black
637 carbon, Science, 337, 1078-1081, https://doi.org/10.1126/science.1223447, 2012.

638 Cappa, C. D., Lim, C. Y., Hagan, D. H., and Kroll, J. H.: Measurements from the Fire Influence
639 on Regional and Global Environments Experiment (FIREX) Fire Lab Mini Chamber Experiment,
640 UC Davis DASH, Dataset, version 1, https://doi.org/10.25338/B8CK5N, 2019a.

641 Cappa, C. D., Zhang, X., Russell, L. M., Collier, S., Lee, A. K. Y., Chen, C.-L., Betha, R., Chen,
642 S., Liu, J., Price, D. J., Sanchez, K. J., McMeeking, G., Williams, L. R., Onasch, T. B., Worsnop,
643 D. R., Abbatt, J., and Zhang, Q.: Light absorption by ambient black and brown carbon and its
644 dependence on black carbon coating state for two California, USA cities in winter and summer,
645 Journal of Geophysical Research-Atmospheres, https://doi.org/10.1029/2018JD029501, 2019b.

646 Chakrabarty, R. K., Moosmüller, H., Chen, L. W. A., Lewis, K., Arnott, W. P., Mazzoleni, C.,
647 Dubey, M. K., Wold, C. E., Hao, W. M., and Kreidenweis, S. M.: Brown carbon in tar balls from
648 smoldering biomass combustion, Atmospheric Chemistry and Physics, 10, 6363-6370,
649 https://doi.org/10.5194/acp-10-6363-2010, 2010.

650 Chakrabarty, R. K., and Heinson, W. R.: Scaling Laws for Light Absorption Enhancement Due to
651 Nonrefractory Coating of Atmospheric Black Carbon Aerosol, Physical Review Letters, 121,
652 218701, https://doi.org/10.1103/PhysRevLett.121.218701, 2018.

653 Chen, Y., and Bond, T. C.: Light absorption by organic carbon from wood combustion, Atmos.
654 Chem. Phys., 10, 1773-1787, https://doi.org/10.5194/acp-10-1773-2010, 2010.

655 Coggon, M. M., Lim, C. Y., Koss, A. R., Sekimoto, K., Yuan, B., Cappa, C. D., Kroll, J. H.,
656 Selimovic, V., Zarzana, K. J., Brown, S. S., Roberts, J. M., Müller, M., Yokelson, R. J., Wisthaler,
657 A., Krechmer, J., Jimenez, J. L., De Gouw, J., and Warneke, C.: OH-chemistry of volatile organic
658 compounds emitted from laboratory and ambient biomass burning smoke: Influence of furans and
659 oxygenated aromatics on ozone and secondary VOC formation., Atmos. Chem. Phys. Discuss.,
660 https://doi.org/10.5194/acp-2019-516, 2019.

661 Collier, S., Williams, L. R., Onasch, T. B., Cappa, C. D., Zhang, X., Russell, L. M., Chen, C.-L.,
662 Sanchez, K. J., Worsnop, D. R., and Zhang, Q.: Influence of emissions and aqueous processing on
663 particles containing black carbon in a polluted urban environment: Insights from a soot particle –
664 aerosol mass spectrometer, Journal of Geophysical Research-Atmospheres, *123*, 6648-6666,
665 https://doi.org/10.1002/2017JD027851, 2018.

666 Cubison, M. J., Ortega, A. M., Hayes, P. L., Farmer, D. K., Day, D., Lechner, M. J., Brune, W. H.,
667 Apel, E., Diskin, G. S., Fisher, J. A., Fuelberg, H. E., Hecobian, A., Knapp, D. J., Mikoviny, T.,

668 Riemer, D., Sachse, G. W., Sessions, W., Weber, R. J., Weinheimer, A. J., Wisthaler, A., and
669 Jimenez, J. L.: Effects of aging on organic aerosol from open biomass burning smoke in aircraft
670 and laboratory studies, Atmos. Chem. Phys., 11, 12049-12064, https://doi.org/10.5194/acp-11-
671 12049-2011, 2011.

672 Fierce, L., Bond, T. C., Bauer, S. E., Mena, F., and Riemer, N.: Black carbon absorption at the
673 global scale is affected by particle-scale diversity in composition, Nat. Comm., 7,
674 https://doi.org/10.1038/ncomms12361, 2016.

675 Forestieri, S. D., Helgestad, T. M., Lambe, A. T., Renbaum-Wolff, L. H., Lack, D. A., Massoli,
676 P., Cross, E. S., Dubey, M. K., Mazzoleni, C., Olfert, J., Freedman, A., Davidovits, P., Onasch, T.
677 B., and Cappa, C. D.: Measurement and modeling of the multi-wavelength optical properties of
678 uncoated flame-generated soot, Atmos. Chem. Phys., 18, 12141-12159,
679 https://doi.org/10.5194/acp-18-12141-2018, 2018.

680 Forrister, H., Liu, J., Scheuer, E., Dibb, J., Ziemba, L., Thornhill, K. L., Anderson, B., Diskin, G.,
681 Perring, A. E., Schwarz, J. P., Campuzano-Jost, P., Day, D. A., Palm, B. B., Jimenez, J. L., Nenes,
682 A., and Weber, R. J.: Evolution of brown carbon in wildfire plumes, Geophysical Research Letters,
683 42, 4623-4630, https://doi.org/10.1002/2015GL063897, 2015.

684 Fuller, K. A., Malm, W. C., and Kreidenweis, S. M.: Effects of mixing on extinction by
685 carbonaceous particles, J. Geophys. Res.-Atmos., 104, 15941-15954,
686 https://doi.org/10.1029/1998jd100069, 1999.

687 Garofalo, L. A., Pothier, M. A., Levin, E. J. T., Campos, T., Kreidenweis, S. M., and Farmer, D.
688 K.: Emission and Evolution of Submicron Organic Aerosol in Smoke from Wildfires in the
689 Western United States, ACS Earth and Space Chem., 3, 1237-1247,
690 https://doi.org/10.1021/acsearthspacechem.9b00125, 2019.

691 Healy, R., Wang, J., Jeong, C. H., Lee, A., Willis, M., Jaroudi, E., Zimmerman, N., Hilker, N.,
692 Murphy, M., and Eckhardt, S.: Light-absorbing properties of ambient black carbon and brown
693 carbon from fossil fuel and biomass burning sources, Journal of Geophysical Research:
694 Atmospheres, 120, 6619-6633, 2015.

695 Hoffer, A., Gelencser, A., Guyon, P., Kiss, G., Schmid, O., Frank, G. P., Artaxo, P., and Andreae,
696 M. O.: Optical properties of humic-like substances (HULIS) in biomass-burning aerosols,
697 Atmospheric Chemistry and Physics, 6, 3563-3570, 2006.

698 Hoffer, A., Tóth, A., Nyirő-Kósa, I., Pósfai, M., and Gelencsér, A.: Light absorption properties of
699 laboratory-generated tar ball particles, Atmos. Chem. Phys., 16, 239-246,
700 https://doi.org/10.5194/acp-16-239-2016, 2016.

701 Hosseini, S., Li, Q., Cocker, D., Weise, D., Miller, A., Shrivastava, M., Miller, J. W., Mahalingam,
702 S., Princevac, M., and Jung, H.: Particle size distributions from laboratory-scale biomass fires
703 using fast response instruments, Atmos. Chem. Phys., 10, 8065-8076, https://doi.org/10.5194/acp-
704 10-8065-2010, 2010.

705 Jacobson, M. Z.: Strong radiative heating due to the mixing state of black carbon in atmospheric
706 aerosols, Nature, 409, 695-697, https://doi.org/10.1038/35055518, 2001.

707 Jen, C. N., Hatch, L. E., Selimovic, V., Yokelson, R. J., Weber, R., Fernandez, A. E., Kreisberg,
708 N. M., Barsanti, K. C., and Goldstein, A. H.: Speciated and total emission factors of particulate

709 organics from burning western U.S. wildland fuels and their dependence on combustion efficiency,
710 Atmos. Chem. Phys., 19, 1013-1026, https://doi.org/10.5194/acp-19-1013-2019, 2019.

711 Kiendler-Scharr, A., Mensah, A. A., Friese, E., Topping, D., Nemitz, E., Prevot, A. S. H., Äijälä,
712 M., Allan, J., Canonaco, F., Canagaratna, M., Carbone, S., Crippa, M., Dall Osto, M., Day, D. A.,
713 De Carlo, P., Di Marco, C. F., Elbern, H., Eriksson, A., Freney, E., Hao, L., Herrmann, H.,
714 Hildebrandt, L., Hillamo, R., Jimenez, J. L., Laaksonen, A., McFiggans, G., Mohr, C., O'Dowd,
715 C., Otjes, R., Ovadnevaite, J., Pandis, S. N., Poulain, L., Schlag, P., Sellegri, K., Swietlicki, E.,
716 Tiitta, P., Vermeulen, A., Wahner, A., Worsnop, D., and Wu, H.-C.: Ubiquity of organic nitrates
717 from nighttime chemistry in the European submicron aerosol, Geophysical Research Letters, 43,
718 7735-7744, https://doi.org/doi:10.1002/2016GL069239, 2016.

719 Kirchstetter, T. W., Novakov, T., and Hobbs, P. V.: Evidence that the spectral dependence of light
720 absorption by aerosols is affected by organic carbon, Journal of Geophysical Research-
721 Atmospheres, 109, D21208, 2004.

722 Kondo, Y., Matsui, H., Moteki, N., Sahu, L., Takegawa, N., Kajino, M., Zhao, Y., Cubison, M. J.,
723 Jimenez, J. L., Vay, S., Diskin, G. S., Anderson, B., Wisthaler, A., Mikoviny, T., Fuelberg, H. E.,
724 Blake, D. R., Huey, G., Weinheimer, A. J., Knapp, D. J., and Brune, W. H.: Emissions of black
725 carbon, organic, and inorganic aerosols from biomass burning in North America and Asia in 2008,
726 J. Geophys. Res., 116, D08204, https://doi.org/10.1029/2010jd015152, 2011.

727 Koss, A. R., Sekimoto, K., Gilman, J. B., Selimovic, V., Coggon, M. M., Zarzana, K. J., Yuan, B.,
728 Lerner, B. M., Brown, S. S., Jimenez, J. L., Krechmer, J., Roberts, J. M., Warneke, C., Yokelson,
729 R. J., and de Gouw, J.: Non-methane organic gas emissions from biomass burning: identification,
730 quantification, and emission factors from PTR-ToF during the FIREX 2016 laboratory experiment,
731 Atmos. Chem. Phys., 18, 3299-3319, https://doi.org/10.5194/acp-18-3299-2018, 2018.

732 Lack, D. A., Cappa, C. D., Cross, E. S., Massoli, P., Ahern, A. T., Davidovits, P., and Onasch, T.
733 B.: Absorption Enhancement of Coated Absorbing Aerosols: Validation of the Photo-Acoustic
734 Technique for Measuring the Enhancement, Aerosol Science and Technology, 43, 1006-1012,
735 https://doi.org/10.1080/02786820903117932, 2009.

736 Lack, D. A., Langridge, J., Bahreni, R., Cappa, C. D., Middlebrook, A., and Schwarz, J. P.: Brown
737 Carbon and Internal Mixing in Biomass Burning Particles, PNAS, 10, 14802-14807,
738 https://doi.org/10.1073/pnas.1206575109, 2012a.

739 Lack, D. A., Richardson, M. S., Law, D., Langridge, J. M., Cappa, C. D., McLaughlin, R. J., and
740 Murphy, D. M.: Aircraft Instrument for Comprehensive Characterization of Aerosol Optical
741 Properties, Part 2: Black and Brown Carbon Absorption and Absorption Enhancement Measured
742 with Photo Acoustic Spectroscopy, Aerosol Science and Technology, 46, 555-568,
743 https://doi.org/10.1080/02786826.2011.645955, 2012b.

744 Lack, D. A., Bahreini, R., Langridge, J. M., Gilman, J. B., and Middlebrook, A. M.: Brown carbon
745 absorption linked to organic mass tracers in biomass burning particles, Atmos. Chem. Phys., 13,
746 2415-2422, https://doi.org/10.5194/acp-13-2415-2013, 2013.

747 Langridge, J. M., Richardson, M. S., Lack, D., Law, D., and Murphy, D. M.: Aircraft Instrument
748 for Comprehensive Characterization of Aerosol Optical Properties, Part I: Wavelength-Dependent
749 Optical Extinction and Its Relative Humidity Dependence Measured Using Cavity Ringdown
750 Spectroscopy, Aerosol Science and Technology, 45, 1305-1318,
751 https://doi.org/10.1080/02786826.2011.592745, 2011.

752 Laskin, A., Lin, P., Laskin, J., Fleming, L. T., and Nizkorodov, S.: Molecular Characterization of
753 Atmospheric Brown Carbon, in: Multiphase Environmental Chemistry in the Atmosphere, ACS
754 Symposium Series, 1299, American Chemical Society, 261-274, 2018.

755 Levin, E. J. T., McMeeking, G. R., Carrico, C. M., Mack, L. E., Kreidenweis, S. M., Wold, C. E.,
756 Moosmüller, H., Arnott, W. P., Hao, W. M., Collett, J. L., and Malm, W. C.: Biomass burning
757 smoke aerosol properties measured during Fire Laboratory at Missoula Experiments (FLAME),
758 Journal of Geophysical Research: Atmospheres, 115, D18210,
759 https://doi.org/10.1029/2009JD013601, 2010.

760 Lim, C. Y., Hagan, D. H., Coggon, M. M., Koss, A. R., Sekimoto, K., De Gouw, J., Warneke, C.,
761 Cappa, C. D., and Kroll, J. H.: Secondary organic aerosol formation from biomass burning
762 emissions, Atmos. Chem. Phys. Discuss., https://doi.org/10.5194/acp-2019-326, 2019.

763 Lin, P., Aiona, P. K., Li, Y., Shiraiwa, M., Laskin, J., Nizkorodov, S. A., and Laskin, A.: Molecular
764 Characterization of Brown Carbon in Biomass Burning Aerosol Particles, Environmental Science
765 & Technology, 50, 11815-11824, https://doi.org/10.1021/acs.est.6b03024, 2016.

766 Liu, D. T., Whitehead, J., Alfarra, M. R., Reyes-Villegas, E., Spracklen, D. V., Reddington, C. L.,
767 Kong, S. F., Williams, P. I., Ting, Y. C., Haslett, S., Taylor, J. W., Flynn, M. J., Morgan, W. T.,
768 McFiggans, G., Coe, H., and Allan, J. D.: Black-carbon absorption enhancement in the atmosphere
769 determined by particle mixing state, Nat. Geosci., 10, 184-U132,
770 https://doi.org/10.1038/ngeo2901, 2017.

771 Liu, S., Aiken, A. C., Arata, C., Dubey, M. K., Stockwell, C. E., Yokelson, R. J., Stone, E. A.,
772 Jayarathne, T., Robinson, A. L., DeMott, P. J., and Kreidenweis, S. M.: Aerosol single scattering
773 albedo dependence on biomass combustion efficiency: Laboratory and field studies, Geophysical
774 Research Letters, 2013GL058392, https://doi.org/10.1002/2013GL058392, 2013.

775 Liu, S., Aiken, A. C., Gorkowski, K., Dubey, M. K., Cappa, C. D., Williams, L. R., Herndon, S.
776 C., Massoli, P., Fortner, E. C., Chhabra, P. S., Brooks, W. A., Onasch, T. B., Worsnop, D. R.,
777 China, S., Sharma, N., Mazzoleni, C., Xu, L., L., N. N., Liu, D., Allan, J. D., Lee, J. D., Fleming,
778 Z. L., Mohr, C., Zotter, P., Szidat, S., and Prevot, A. S. H.: Enhanced light absorption by mixed
779 source black and brown carbon particles in UK winter, Nat. Comm., 6, 8435,
780 https://doi.org/10.1038/ncomms9435, 2015.

781 Mann, G. W., Carslaw, K. S., Reddington, C. L., Pringle, K. J., Schulz, M., Asmi, A., Spracklen,
782 D. V., Ridley, D. A., Woodhouse, M. T., Lee, L. A., Zhang, K., Ghan, S. J., Easter, R. C., Liu, X.,
783 Stier, P., Lee, Y. H., Adams, P. J., Tost, H., Lelieveld, J., Bauer, S. E., Tsigaridis, K., van Noije,
784 T. P. C., Strunk, A., Vignati, E., Bellouin, N., Dalvi, M., Johnson, C. E., Bergman, T., Kokkola,
785 H., von Salzen, K., Yu, F., Luo, G., Petzold, A., Heintzenberg, J., Clarke, A., Ogren, J. A., Gras,
786 J., Baltensperger, U., Kaminski, U., Jennings, S. G., O'Dowd, C. D., Harrison, R. M., Beddows,
787 D. C. S., Kulmala, M., Viisanen, Y., Ulevicius, V., Mihalopoulos, N., Zdimal, V., Fiebig, M.,
788 Hansson, H. C., Swietlicki, E., and Henzing, J. S.: Intercomparison and evaluation of global
789 aerosol microphysical properties among AeroCom models of a range of complexity, Atmos. Chem.
790 Phys., 14, 4679-4713, https://doi.org/10.5194/acp-14-4679-2014, 2014.

791 May, A. A., McMeeking, G. R., Lee, T., Taylor, J. W., Craven, J. S., Burling, I., Sullivan, A. P.,
792 Akagi, S., Collett Jr., J. L., Flynn, M., Coe, H., Urbanski, S. P., Seinfeld, J. H., Yokelson, R. J.,
793 and Kreidenweis, S. M.: Aerosol emissions from prescribed fires in the United States: A synthesis

of laboratory and aircraft measurements, Journal of Geophysical Research: Atmospheres, 119, 11,826-811,849, https://doi.org/10.1002/2014JD021848, 2014.

McMeeking, G. R., Kreidenweis, S. M., Baker, S., Carrico, C. M., Chow, J. C., Collett, J. L., Hao, W. M., Holden, A. S., Kirchstetter, T. W., Malm, W. C., Moosmüller, H., Sullivan, A. P., and Wold, C. E.: Emissions of trace gases and aerosols during the open combustion of biomass in the laboratory, Journal of Geophysical Research: Atmospheres, 114, D19210, https://doi.org/10.1029/2009JD011836, 2009.

McMeeking, G. R., Fortner, E., Onasch, T. B., Taylor, J. W., Flynn, M., Coe, H., and Kreidenweis, S. M.: Impacts of nonrefractory material on light absorption by aerosols emitted from biomass burning, Journal of Geophysical Research: Atmospheres, 119, 12,272-212,286, https://doi.org/10.1002/2014JD021750, 2014.

Metcalf, A. R., Loza, C. L., Coggon, M. M., Craven, J. S., Jonsson, H. H., Flagan, R. C., and Seinfeld, J. H.: Secondary Organic Aerosol Coating Formation and Evaporation: Chamber Studies Using Black Carbon Seed Aerosol and the Single-Particle Soot Photometer, Aerosol Sci. Technol., 47, 326-347, https://doi.org/10.1080/02786826.2012.750712, 2013.

Mohr, C., Lopez-Hilfiker, F. D., Zotter, P., Prévôt, A. S. H., Xu, L., Ng, N. L., Herndon, S. C., Williams, L. R., Franklin, J. P., Zahniser, M. S., Worsnop, D. R., Knighton, W. B., Aiken, A. C., Gorkowski, K. J., Dubey, M. K., Allan, J. D., and Thornton, J. A.: Contribution of Nitrated Phenols to Wood Burning Brown Carbon Light Absorption in Detling, United Kingdom during Winter Time, Environmental Science & Technology, 47, 6316-6324, https://doi.org/10.1021/es400683v, 2013.

Onasch, T. B., Trimborn, A. M., Fortner, E. C., Jayne, J. T., Kok, G. L., Williams, L. R., Davidovits, P., and Worsnop, D. R.: Soot Particle Aerosol Mass Spectrometer: Development, Validation and Initial Application, Aerosol Science and Technology, 46, 804-817, https://doi.org/10.1080/02786826.2012.663948, 2012.

Peng, J., Hu, M., Guo, S., Du, Z., Zheng, J., Shang, D., Zamora, M. L., Zeng, L., Shao, M., Wu, Y.-S., Zheng, J., Wang, Y., Glen, C. R., Collins, D. R., Molina, M. J., and Zhang, R.: Markedly enhanced absorption and direct radiative forcing of black carbon under polluted urban environments, Proc. Natl. Acad. Sci. U. S. A., 113, 4266-4271, https://doi.org/10.1073/pnas.1602310113, 2016.

Phillips, S. M., and Smith, G. D.: Spectroscopic comparison of water- and methanol-soluble brown carbon particulate matter, Aerosol Science and Technology, 51, 1113-1121, https://doi.org/10.1080/02786826.2017.1334109, 2017.

Pokhrel, R. P., Wagner, N. L., Langridge, J. M., Lack, D. A., Jayarathne, T., Stone, E. A., Stockwell, C. E., Yokelson, R. J., and Murphy, S. M.: Parameterization of single-scattering albedo (SSA) and absorption Ångström exponent (AAE) with EC / OC for aerosol emissions from biomass burning, Atmos. Chem. Phys., 16, 9549-9561, https://doi.org/10.5194/acp-16-9549-2016, 2016.

Pokhrel, R. P., Beamesderfer, E. R., Wagner, N. L., Langridge, J. M., Lack, D. A., Jayarathne, T., Stone, E. A., Stockwell, C. E., Yokelson, R. J., and Murphy, S. M.: Relative importance of black carbon, brown carbon, and absorption enhancement from clear coatings in biomass burning emissions, Atmospheric Chemistry and Physics, 17, 5063-5078, https://doi.org/10.5194/acp-17-5063-2017, 2017.

837 Qin, Y. M., Tan, H. B., Li, Y. J., Li, Z. J., Schurman, M. I., Liu, L., Wu, C., and Chan, C. K.:
838 Chemical characteristics of brown carbon in atmospheric particles at a suburban site near
839 Guangzhou, China, Atmos. Chem. Phys., 18, 16409-16418, https://doi.org/10.5194/acp-18-16409-
840 2018, 2018.

841 Reid, J. S., Koppmann, R., Eck, T. F., and Eleuterio, D. P.: A review of biomass burning emissions
842 part II: intensive physical properties of biomass burning particles, Atmos. Chem. Phys., 5, 799-
843 825, https://doi.org/10.5194/acp-5-799-2005, 2005.

844 Sahu, L. K., Kondo, Y., Moteki, N., Takegawa, N., Zhao, Y., Cubison, M. J., Jimenez, J. L., Vay,
845 S., Diskin, G. S., Wisthaler, A., Mikoviny, T., Huey, L. G., Weinheimer, A. J., and Knapp, D. J.:
846 Emission characteristics of black carbon in anthropogenic and biomass burning plumes over
847 California during ARCTAS-CARB 2008, Journal of Geophysical Research-Atmospheres, 117,
848 https://doi.org/10.1029/2011jd017401, 2012.

849 Saleh, R., Hennigan, C. J., McMeeking, G. R., Chuang, W. K., Robinson, E. S., Coe, H., Donahue,
850 N. M., and Robinson, A. L.: Absorptivity of brown carbon in fresh and photo-chemically aged
851 biomass-burning emissions, Atmospheric Chemistry and Physics, 13, 7683-7693,
852 https://doi.org/10.5194/acp-13-7683-2013, 2013.

853 Saleh, R., Robinson, E. S., Tkacik, D. S., Ahern, A. T., Liu, S., Aiken, A. C., Sullivan, R. C.,
854 Presto, A. A., Dubey, M. K., Yokelson, R. J., Donahue, N. M., and Robinson, A. L.: Brownness
855 of organics in aerosols from biomass burning linked to their black carbon content, Nature Geosci,
856 7, 647-650, https://doi.org/10.1038/ngeo2220, 2014.

857 Saleh, R., Cheng, Z., and Atwi, K.: The Brown–Black Continuum of Light-Absorbing Combustion
858 Aerosols, Environmental Science & Technology Letters, ASAP,
859 https://doi.org/10.1021/acs.estlett.8b00305, 2018.

860 Schneider, J., Weimer, S., Drewnick, F., Borrmann, S., Helas, G., Gwaze, P., Schmid, O., Andreae,
861 M. O., and Kirchner, U.: Mass spectrometric analysis and aerodynamic properties of various types
862 of combustion-related aerosol particles, International Journal of Mass Spectrometry, 258, 37-49,
863 https://doi.org/10.1016/j.ijms.2006.07.008, 2006.

864 Schwarz, J. P., Gao, R. S., Spackman, J. R., Watts, L. A., Thomson, D. S., Fahey, D. W., Ryerson,
865 T. B., Peischl, J., Holloway, J. S., Trainer, M., Frost, G. J., Baynard, T., Lack, D. A., de Gouw, J.
866 A., Warneke, C., and Del Negro, L. A.: Measurement of the mixing state, mass, and optical size
867 of individual black carbon particles in urban and biomass burning emissions, Geophysical
868 Research Letters, 35, L13810, https://doi.org/10.1029/2008gl033968, 2008.

869 Sekimoto, K., Koss, A. R., Gilman, J. B., Selimovic, V., Coggon, M. M., Zarzana, K. J., Yuan, B.,
870 Lerner, B. M., Brown, S. S., Warneke, C., Yokelson, R. J., Roberts, J. M., and de Gouw, J.: High-
871 and low-temperature pyrolysis profiles describe volatile organic compound emissions from
872 western US wildfire fuels, Atmos. Chem. Phys., 18, 9263-9281, https://doi.org/10.5194/acp-18-
873 9263-2018, 2018.

874 Sengupta, D., Samburova, V., Bhattarai, C., Kirillova, E., Mazzoleni, L., Iaukea-Lum, M., Watts,
875 A., Moosmüller, H., and Khlystov, A.: Light absorption by polar and non-polar aerosol compounds
876 from laboratory biomass combustion, Atmos. Chem. Phys., 18, 10849-10867,
877 https://doi.org/10.5194/acp-18-10849-2018, 2018.

878 Shamjad, P. M., Tripathi, S. N., Thamban, N. M., and Vreeland, H.: Refractive Index and
879 Absorption Attribution of Highly Absorbing Brown Carbon Aerosols from an Urban Indian City-
880 Kanpur, Scientific Reports, 6, 37735, https://doi.org/10.1038/srep37735, 2016.

881 Shiraiwa, M., Kondo, Y., Iwamoto, T., and Kita, K.: Amplification of Light Absorption of Black
882 Carbon by Organic Coating, Aerosol Science and Technology, 44, 46-54,
883 https://doi.org/10.1080/02786820903357686, 2010.

884 Sumlin, B. J., Pandey, A., Walker, M. J., Pattison, R. S., Williams, B. J., and Chakrabarty, R. K.:
885 Atmospheric Photooxidation Diminishes Light Absorption by Primary Brown Carbon Aerosol
886 from Biomass Burning, Environmental Science & Technology Letters, 4, 540-545,
887 https://doi.org/10.1021/acs.estlett.7b00393, 2017.

888 Sumlin, B. J., Heinson, Y. W., Shetty, N., Pandey, A., Pattison, R. S., Baker, S., Hao, W. M., and
889 Chakrabarty, R. K.: UV–Vis–IR spectral complex refractive indices and optical properties of
890 brown carbon aerosol from biomass burning, Journal of Quantitative Spectroscopy and Radiative
891 Transfer, 206, 392-398, https://doi.org/10.1016/j.jqsrt.2017.12.009, 2018.

892 Wandinger, Ulla, Müller, Detlef, Böckmann, Christine, Althausen, Dietrich, Matthias, Volker,
893 Bösenberg, Jens, Weiß, Volker, Fiebig, Markus, Wendisch, Manfred, Stohl, Andreas, and
894 Ansmann, A.: Optical and microphysical characterization of biomass- burning and industrial-
895 pollution aerosols from- multiwavelength lidar and aircraft measurements, Journal of Geophysical
896 Research: Atmospheres, 107, LAC 7-1-LAC 7-20, https://doi.org/doi:10.1029/2000JD000202,
897 2002.

898 Washenfelder, R. A., Attwood, A. R., Brock, C. A., Guo, H., Xu, L., Weber, R. J., Ng, N. L., Allen,
899 H. M., Ayres, B. R., Baumann, K., Cohen, R. C., Draper, D. C., Duffey, K. C., Edgerton, E., Fry,
900 J. L., Hu, W. W., Jimenez, J. L., Palm, B. B., Romer, P., Stone, E. A., Wooldridge, P. J., and
901 Brown, S. S.: Biomass burning dominates brown carbon absorption in the rural southeastern
902 United States, Geophysical Research Letters, 42, 653-664,
903 https://doi.org/10.1002/2014GL062444, 2015.

904 Xie, M., Hays, M. D., and Holder, A. L.: Light-absorbing organic carbon from prescribed and
905 laboratory biomass burning and gasoline vehicle emissions, Scientific Reports, 7, 7318,
906 https://doi.org/10.1038/s41598-017-06981-8, 2017.

907 Yang, M., Howell, S. G., Zhuang, J., and Huebert, B. J.: Attribution of aerosol light absorption to
908 black carbon, brown carbon, and dust in China – interpretations of atmospheric measurements
909 during EAST-AIRE, Atmospheric Chemistry and Physics, 9, 2035-2050,
910 https://doi.org/10.5194/acp-9-2035-2009, 2009.

911 Zhang, X., Kim, H., Parworth, C., Young, D. E., Zhang, Q., Metcalf, A. R., and Cappa, C. D.:
912 Optical Properties of Wintertime Aerosols from Residential Wood Burning in Fresno, CA: Results
913 from DISCOVER-AQ 2013, Environmental Science & Technology, 50, 1681-1690,
914 https://doi.org/10.1021/acs.est.5b04134, 2016.

915

916

9 Tables

Table 1. Fuels by particle Class.

Class	Fuel	SSA range	[OA]/[BC] range
Class 1	Chaparral, canopy, litter (pine), building materials, excelsior	0.23-0.43	0.3-2.4
Class 2	Manzanita, Sage, litter (fir)	0.43-0.60	1.5-4.1
Type 3	Pine, fir, litter, canopy, juniper	0.60-0.74	6.6-20
Class 4	Pine, fir, canopy, rotten log, ceonothos	0.74-0.87	8.3-55
Class 5	Canopy (pine), rice, bear grass, duff	0.87-0.93	31-143
Class 6	Rotten log, duff, peat, dung	0.93-1.00	431-10^5

10 Figures

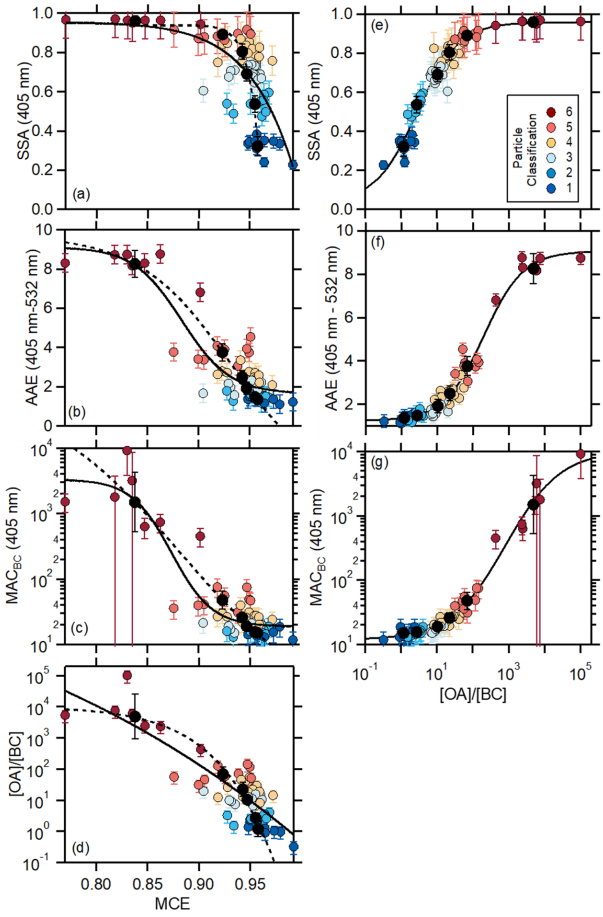

Figure 1. (left panels) Relationship between (a) the SSA_{405nm}, (b) the $AAE_{405\text{-}532}$, (c) the MAC_{BC}, and (d) the [OA]/[BC] mass ratio and the modified combustion efficiency, MCE. Results for individual burns are shown as points colored by the particle Class, and Class average values are shown as black circles. Uncertainties on the Class averages are 1σ based on measurement variability and uncertainties on for the individual burns are from error propagation of measurement uncertainties. The solid black lines are fits to the individual burns (colored points) while the dashed black lines are fits to the Class averages (Table S2). (right panels) Relationship between (e) the SSA_{405nm}, (f) the $AAE_{405\text{-}532}$, and (g) the MAC_{BC} on the [OA]/[BC] mass ratio. The solid black lines here are sigmoidal fits to the individual burns. Fits to the Class averages are similar.

933

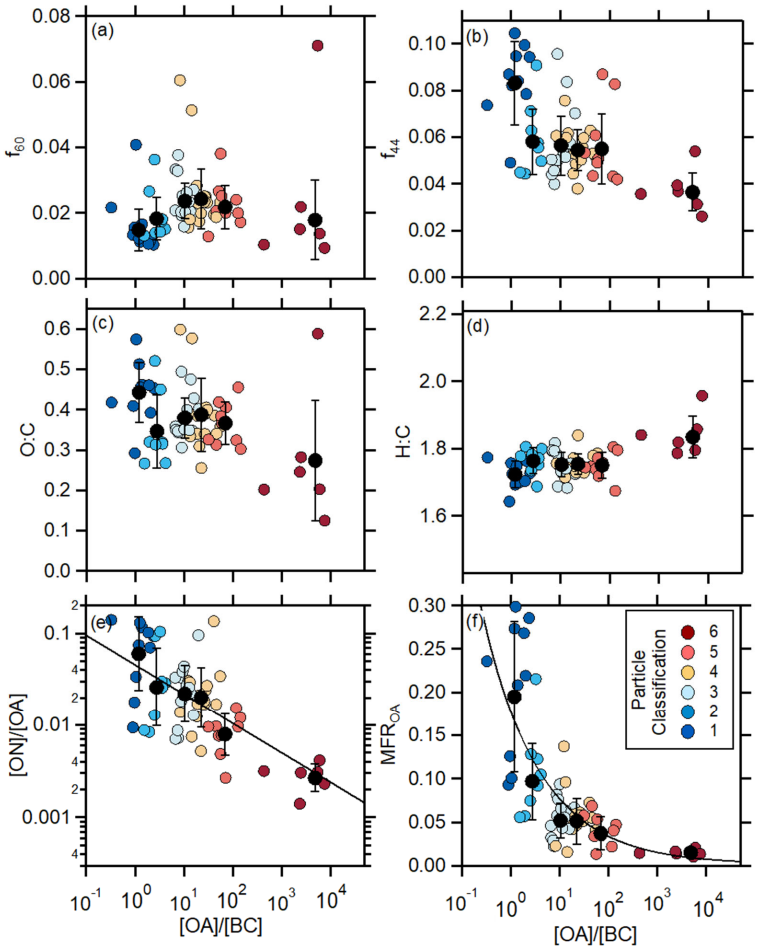

934

935 **Figure 2**. Dependence of (a) f_{60}, (b) f_{44}, (c) O:C, (d) H:C, (e) the nitrated organic fraction of OA,
936 $f_{ON\text{-}OA}$, and (f) the OA volatility, characterized as the mass fraction remaining after heating. Results
937 for individual burns are shown as points colored by the particle Class, and Class average values
938 are shown as black circles. Uncertainties on the Class averages are 1σ based on measurement
939 variability. For $f_{ON\text{-}OA}$ and MFR_{OA}, fits to the observations are shown (see text).

940

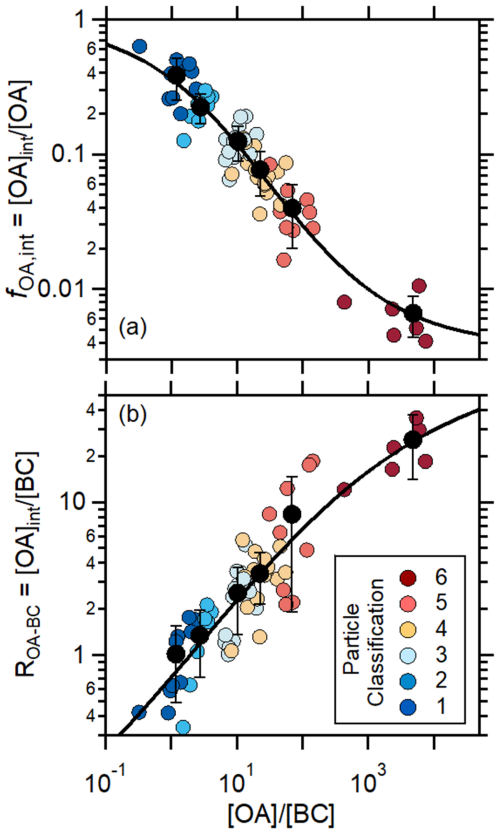

941

942 **Figure 3.** Relationship between (a) the fraction of OA that is internally mixed with BC, $f_{OA,int}$ and
943 (b) the OA-to-BC mass ratio for only the internally mixed OA, and the total [OA]/[BC] mass ratio.
944 Results for individual burns are shown as points colored by the particle Class, and Class average
945 values are shown as black circles. Uncertainties on the Class averages are 1σ based on
946 measurement variability. Black lines are sigmoidal fits to the data, in log-log space.

947

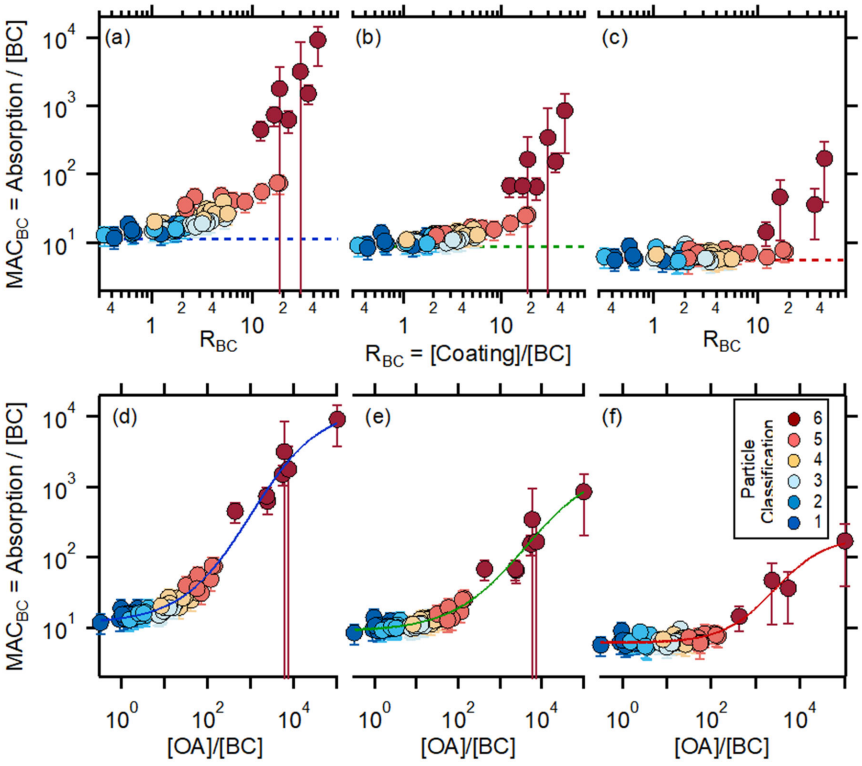

Figure 4. (Top Panels) The relationship between the wavelength-specific MAC_{BC} and the coating-to-BC mass ratio for (a) 405 nm, (b) 532 nm and (c) 781 nm. The horizontal dashed lines show the derived $MAC_{BC,pure}$ values. (Bottom Panels) The relationship between the wavelength-dependent MAC_{BC} and the total [OA]/[BC] mass ratio for (d) 405 nm, (e) 532 nm and (f) 781 nm. The lines are sigmoidal fits. Uncertainties for the individual burns are determined from error propagation. Graphs of the wavelength-specific MAC_{BC} versus [OA]/[BC] with each shown using independent y-axis scales are provided for comparison in Figure S1.

Deleted: Figure S1

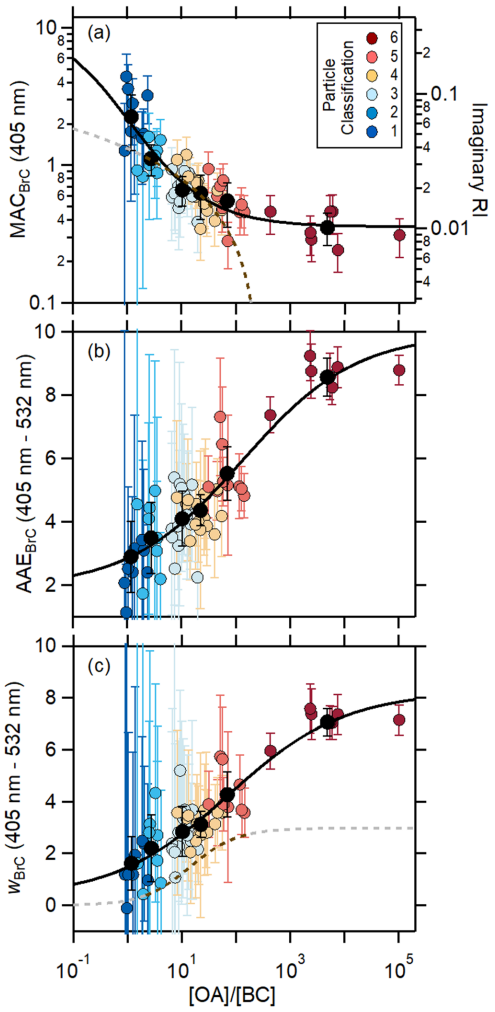

958

959 **Figure 5.** Relationship between (a) $MAC_{BrC,405nm}$, (b) $AAE_{BrC,405-532}$, and (c) $w_{BrC,405-532}$ and the
960 [OA]/[BC] mass ratio. The solid lines are sigmoidal fits to the observations, against
961 log([OA]/[BC]). The dashed lines are based on the parameterization of Saleh et al. (2014), with
962 the brown color indicating the measuring range in that study and the gray color extrapolated.
963 Results for individual burns are shown as points colored by the particle Class, and Class average
964 values are shown as black circles. Uncertainties on the Class averages are 1σ based on
965 measurement variability. Uncertainties for the individual burns are determined from error
966 propagation.

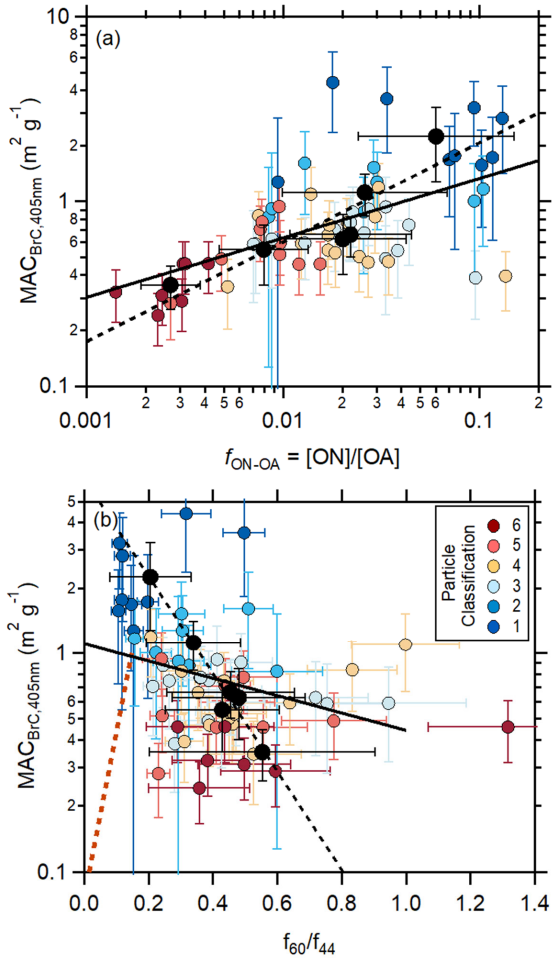

Figure 6. Relationship between the $MAC_{BrC,405nm}$ and (a) the nitrated organic fraction of total organic aerosol, f_{ON-OA}, and (b) the f_{60}/f_{44} ion ratio for organic aerosol. Results for individual burns are shown as points colored by the particle Class, and Class average values are shown as black circles. Uncertainties on the Class averages are 1σ based on measurement variability. Uncertainties for the individual burns are determined from error propagation. Solid black lines are fits to all burns and dashed black lines are fits to the Class averages. The dashed brown line in panel (b) is the relationship reported by Lack et al. (2013) for ambient particles in a biomass burning plume.

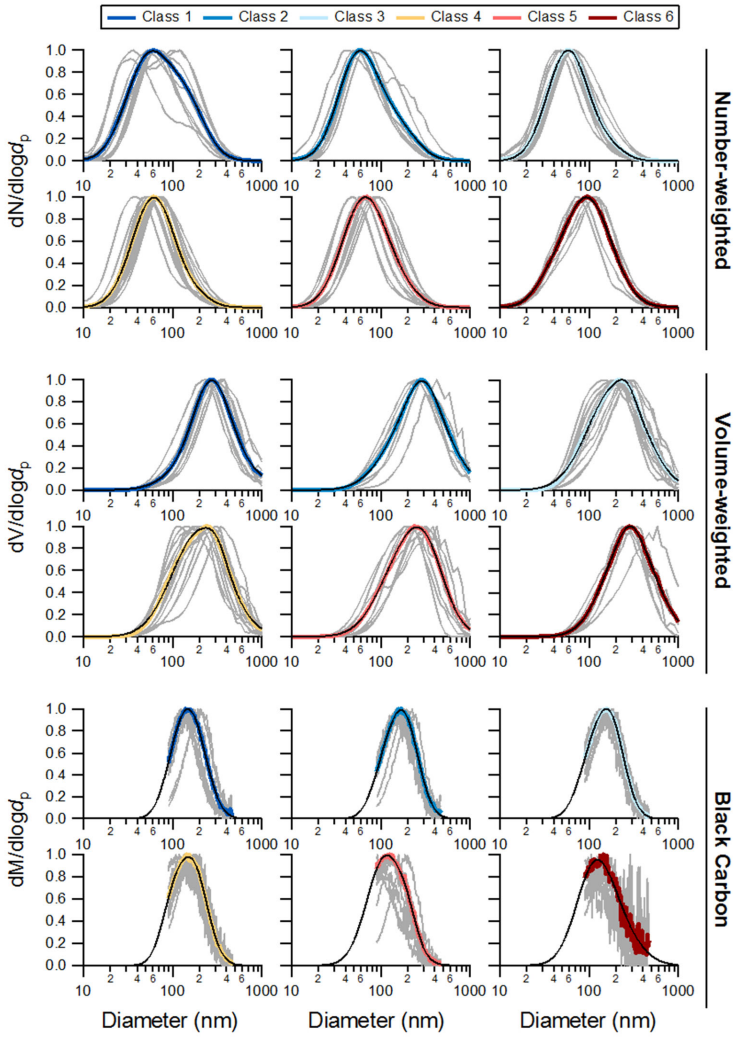

Figure 7. Class-specific total particle number-weighted (top) and volume-weighted (middle) mobility size distributions, and the BC-only mass-weighted (bottom) size distribution. Individual burns are shown in gray and class averages are shown as colors. Bimodal log-normal fits are thin black lines. Note that the number-weighted and volume-weighted distributions are graphed versus mobility diameter and the BC mass-weighted distribution against the BC volume equivalent diameter.

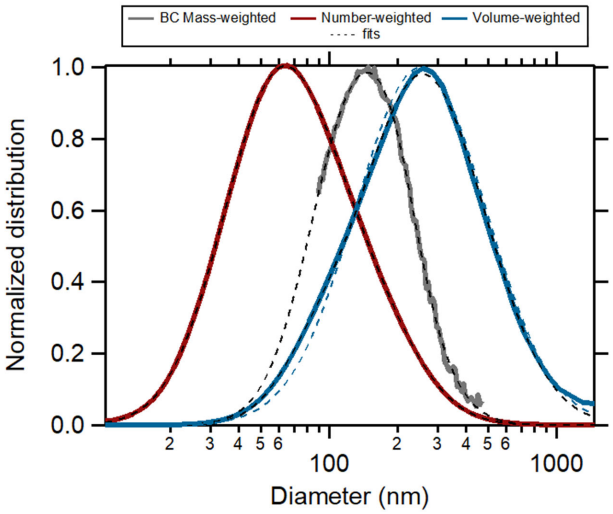

Figure 8. Average total particle number-weighted (red) and volume-weighted (blue) size distributions and the BC-specific mass-weighted size distributions. Black dashed lines are bimodal log-normal fits. The dashed blue line is the total particle volume-weighted distribution calculated from a single-mode fit to the number-weighted distribution. Note that the number-weighted and volume-weighted distributions are graphed versus mobility diameter and the BC mass-weighted distribution against the BC volume equivalent diameter.

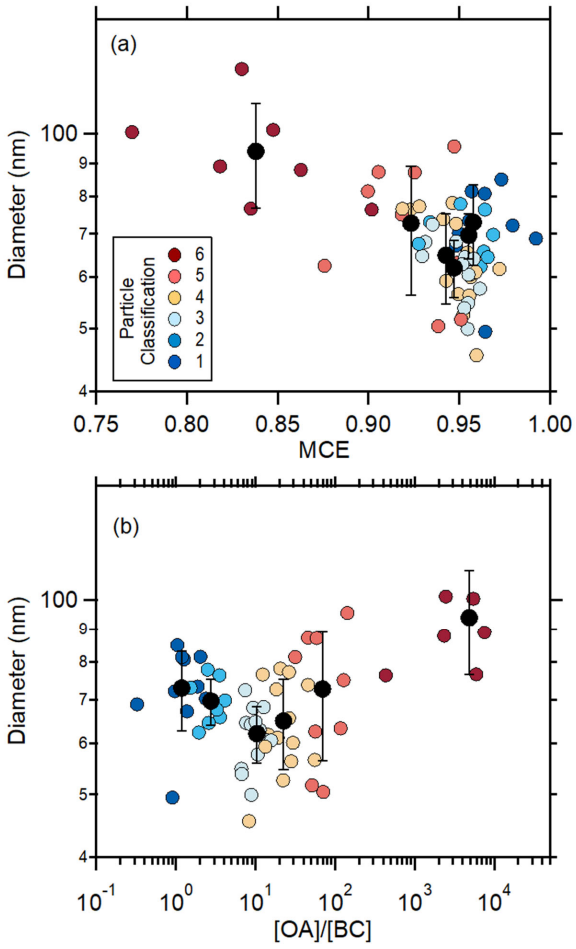

992

993 **Figure 9.** Relationship between number-weighted particle median diameter and (a) the MCE and
994 (b) the [OA]/[BC] ratio. Colored circles are for individual burns and black circles for particle class
995 averages.

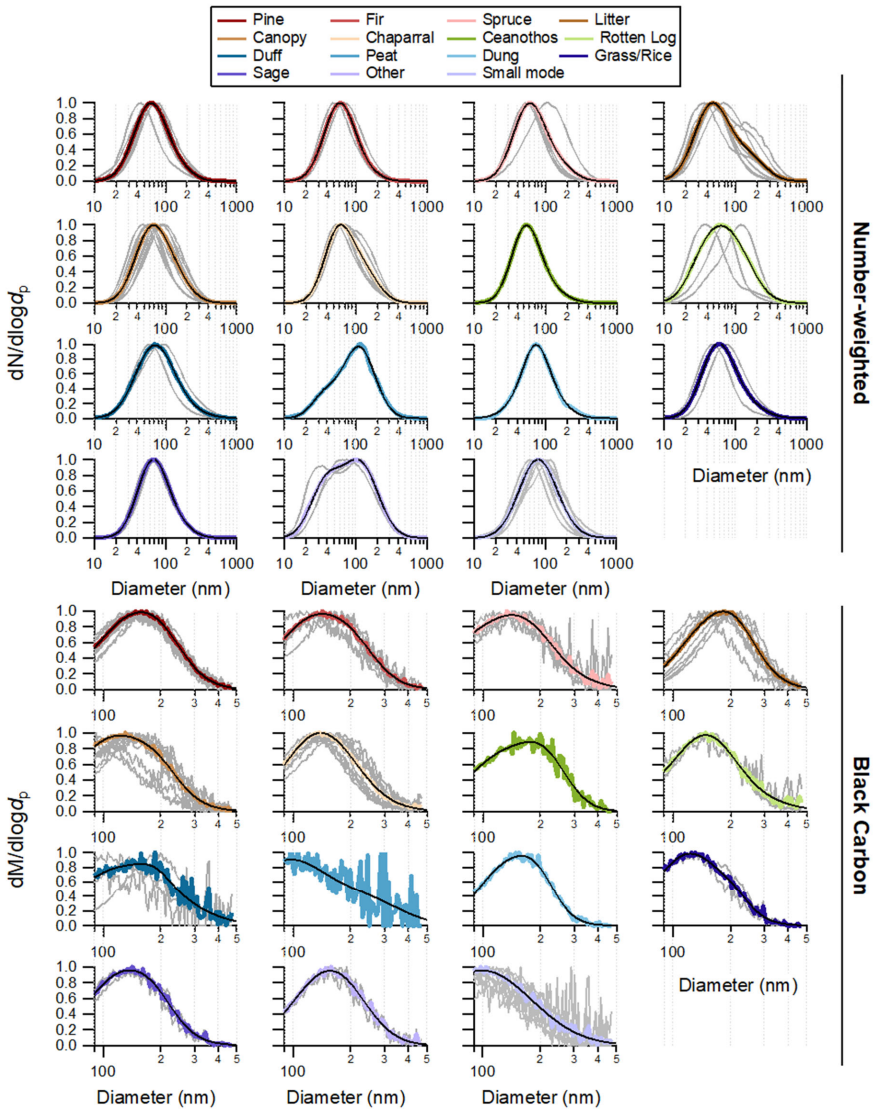

Figure 10. Normalized total particle number-weighted (top) and the BC-only mass-weighted (bottom) size distributions shown by fuel type (see legend). Individual burns are gray and averages for a fuel type colors. For some fuels there is only one size distribution. Bimodal log-normal fits are the black lines. The "other" category includes non-traditional biofuels, specifically building materials and excelsior.

Supplementary Material for:

Biomass-burning derived particles from a wide variety of fuels: Part 1: Properties of primary particles

Crystal D. McClure[1], Christopher Y. Lim[2,%], David H. Hagan[2], Jesse H. Kroll[2], Christopher D. Cappa[1,3,*]

[1] Department of Civil and Environmental Engineering, University of California, Davis, CA 95616

[2] Department of Civil and Environmental Engineering, Massachusetts Institute of Technology, Cambridge, MA, USA

[3] Atmospheric Sciences Graduate Group, University of California, Davis, CA, USA 95616

[%] Now at Department of Chemistry, University of Toronto, Ontario, Canada

[*] To whom correspondence should be addressed: cdcappa@ucdavis.edu

10.1 Description of Instrumentation

Particle Optical Property Measurements

Particle optical properties for PM_1 were measured at 405 nm and 532 nm using the UC Davis Cavity Ringdown-Photoacoustic Spectrometer (CRD-PAS). In the UC Davis CRD-PAS, Light absorption coefficients (b_{abs}; units = Mm^{-1}) for dry particles are determined using photoacoustic spectroscopy (Lack et al., 2012b). Light extinction coefficients (b_{ext}; units = Mm^{-1}) for dry (<20% relative humidity) particles are measured at 405 nm and 532 nm via cavity ringdown spectroscopy (Langridge et al., 2011). Humidified light extinction measurements (RH ~85%) are also measured at 532 nm by cavity ringdown spectroscopy. The absorption measurements from the PAS were calibrated relative to the extinction measurement from the CRD using gas-phase O_3 and NO_2 with an estimated accuracy of 5% at 532 nm and 8% at 405 nm. Light absorption and scattering coefficients were also measured at 781 nm using a commercial PASS-3 photoacoustic spectrometer (DMT, Inc.). In the PASS-3, light absorption coefficients are measured by photoacoustic spectroscopy. Light scattering coefficients (b_{sca}; units = Mm^{-1}) are determined for dry particles with the PASS-3 using reciprocal nephelometry. The absorption measured by the

PASS-3 was calibrated relative to the UC Davis PAS using polydisperse fullerene soot and assuming that the absorption Ångstrom exponent was 1.4 (Metcalf et al., 2013). The estimated uncertainty in b_{abs} at 781 nm is 10%.

Particle Composition Measurements

Refractory black carbon measurement

Refractory black carbon (rBC) concentrations and BC-specific particle size distributions were measured using a single particle soot photometer (SP2). The SP2 measures the concentration of rBC within individual rBC-containing particles. Sampled particles pass through a 1064 nm intracavity laser. Absorption of this light by rBC leads to rapid heating of the particles. If heating outweighs conductive cooling the particles will reach a sufficiently high temperature (i.e. their boiling point) that they will incandesce. The intensity of this incandescent light is proportional to the rBC mass of that particle (usually on the order of 0.1 – 10 fg per particle). Size distributions of only the rBC (exclusive of any other internally mixed material) are generated by converting the per particle mass to a volume equivalent diameter ($d_{p,VED}$ here, assuming ρ_{rBC} = 1.8 g cm^{-3}) and binning the particles by size. The SP2 was calibrated using size-selected fullerene particles (Lot L20W054, Alfa Aesar, Ward Hill, MA, USA).

When the number concentration of rBC-containing or non-rBC-containing particles is large, the SP2 may suffer from negative biases in the concentration measurement. This can happen when the SP2 detectors are triggered by one particle and a second passes through the viewing volume during the detection window (typically ~50 μs). Such particle coincidence effects can be minimized by decreasing the sample flowrate into the SP2 to decrease the likelihood that two particles are simultaneously in the viewing volume. Here, the SP2 sample flowrate was varied from 5 sccm to 120 sccm in a step-wise manner over the course of an experiment to deal with the very large dynamic range of concentrations in the mini chamber. The flow rate was increased to maintain an approximately constant particle count rate in the instrument while minimizing the influence of particle coincidence. Inspection of individual particle detection events indicates that particle coincidence was generally avoided.

The SP2 data were processed using the SP2 Toolkit from the Paul Scherer Institute (PSI), developed by Martin Gysel. The SP2 size-dependent counting efficiency was determined by

simultaneously measuring the concentration of the calibration particles with a mixing condensation particle counter (BMI Model 2002). The particle counting efficiency was found to be unity for particles with $d_{p,VED} > 100$ nm. The SP2 used in this study measured particles over the size range $90 \leq d_{p,VED} \leq 822$. Below the lower size limit, the detection efficiency falls off rapidly due, in part, to the large surface area-to-volume (SA-to-V) ratio of these particles. When the SA-to-V ratio is sufficiently large conductive cooling competes effectively with the radiative heating from the laser and the particles do not emit enough incandescent light at short enough wavelengths to trigger detection. Above the upper size limit, the incandescence level is sufficient to saturate the detector, leading to an underestimate in particle mass. All SP2 mass concentration measurements were corrected for the missing mass contained in particles below the lower and upper size limit, using a multi-mode fitting approach.

The observed campaign average distribution mode peak is around 150 nm. The observed distributions (1 min averages) were fit to a four-mode log-normal distribution to estimate and correct for the rBC outside of the SP2 detection window, i.e. for rBC "missing mass". The average ratio between the observed rBC concentration and the total estimated from fitting was 0.83 ± 0.06 (1σ). There was some experiment-to-experiment and time-dependent variability in the missing mass fraction that is accounted for by fitting the observations at 1 min time resolution. This approach follows that of Zhang et al. (2016). While a single mode fit provides a reasonably representation of the overall campaign average distribution, inspection of the individual distributions across the experiments indicates that a multi-mode fitting approach provides a substantially more robust description of the observed size distribution, especially as particle aging proceeds.

Composition and concentration of NR-PM

The concentration of non-refractory particulate matter (NR-PM) species in PM_1 were measured using a high-resolution time-of-flight aerosol mass spectrometer (HR-ToF-AMS, henceforth HR-AMS) (Canagaratna et al., 2007) during both the Fresno and Fontana studies, as discussed in detail by (Lim et al., 2019). The NR-PM components are functionally defined as those materials that evaporate rapidly after impaction onto a heated surface *in vacuo* at ~600 °C. The NR-PM components characterized include particulate sulfate, nitrate, ammonium, chloride and organic matter. The data were processed using the PIKA toolkit in IGOR (Wavemetrics, Inc.). The

collection efficiency (CE) of the HR-AMS was determined by comparison with size distributions measured using the scanning electrical mobility spectrometer (SEMS). The collection efficiency differed between primary and secondary and secondary particles and was found to co-vary with the volatility of the organic aerosol. The variation in the CE was empirically accounted for, as discussed in (Lim et al., 2019). The estimated uncertainty for the HR-AMS measurements is ±30%, although the precision is much better than this.

Particulate nitrated organics characterization

The concentration of nitrated organic functional groups (ON_f) is determined from the HR-AMS measurements. Kiendler-Scharr et al. (2016) showed that the fraction of total nitrate measured by the HR-AMS that derives from organic nitrate functional groups ($f_{ON\text{-}N}$) relates to the measured $[NO_2^+]/[NO^+]$ ratio (R_{meas}):

$$f_{ON-N} = \frac{(1+R_{ON})\cdot(R_{meas}-R_{calib})}{(1+R_{meas})\cdot(R_{ON}-R_{calib})} \quad \text{(S1)}$$

where R_{ON} = 0.1 and R_{calib} is an instrument-specific factor determined from calibration with NH_4NO_3 and here equaling 0.45. The Kiendler-Scharr et al. (2016) approach focused on the behavior of organic nitrates. We assume here that nitro-organics behave similarly and thus that ON_f encompasses contributions from both nitrate and nitro functional groups. Equation S1 is thought reliable when the $f_{ON\text{-}N} > 0.15$ (Bruns et al., 2010). The average $f_{ON\text{-}N}$ for the FIREX measurements is 0.74 ± 0.24 (1σ). The concentration of particulate ON functional groups is then $[ON_f] = f_{ON\text{-}N}\cdot[NO_3^-]$. Note that this includes only the mass of the functional group; the total mass concentration of the ON species (including the carbon backbone) can be estimated by multiplying the ON_f concentration by the ratio between an assumed MW for the ON species and that for the nitrate functional group. We assume that ON species have a MW = 200 amu, and thus $[ON] = 3.22\cdot[ON_f]$. If the ON signal is dominated by nitro functional groups, rather than nitrate, then the estimated [ON] is a lower limit.

Composition and concentration of BC-containing particles

The concentrations and composition of only BC-containing particles were determined using a soot particle aerosol mass spectrometer (SP-AMS) (Onasch et al., 2012). In the SP-AMS, a focused particle beam is intersected with an intra-cavity Nd:YAG laser operating at 1064 nm. Particles

containing BC are rapidly heated by the laser, leading to evaporation of both the NR-PM materials and the refractory BC. In these studies, the standard HR-AMS tungsten vaporizer was removed so that particles that do not contain BC are not vaporized and are therefore not detected. Thus, the SP-AMS is specific to BC-containing particles, as operated here. In addition to BC, the SP-AMS measures the internally mixed particulate inorganic (sulfate, nitrate, ammonium, and chloride) and organic mass loading. The NR-PM species that are associated with BC will be distinguished from the bulk average NR-PM species (from the HR-AMS) using the subscript BC (i.e. NR-PM_{rBC}). The SP-AMS particle detection efficiency is determined in large part by the extent of overlap between the particle and laser beam. Particles were sampled through a PM_1 aerodynamic lens, with particles measured down to ~40 nm vacuum aerodynamic diameter. The SP-AMS detection efficiency was determined by referencing the rBC concentration measured by the SP-AMS to that measured by the SP2, as in (Collier et al., 2018). The SP-AMS/SP2 ratio depended on the ratio between the NR-PM_{BC} and BC, with the NR-PM/rBC ratio decreasing as the SP-AMS/SP2 ratio increases. However, throughout this work we use only the [NR-PM_{rBC}]/[rBC] or [OA_{rBC}]/[rBC] ratios, which are not dependent on the absolute instrument calibration, but only the relative detection efficiency of these species. The coating-to-core mass ratio for both campaigns is calculated directly from the SP-AMS measurements as R_{BC} = [NR-PM]$_{BC}$/[BC].

Gas Composition Measurements

The concentrations of select gas-phase non-methane organic gases (NMOG) and some inorganic species (e.g. HONO) were measured using H_3O^+ and I^- chemical ionization mass spectrometers (CIMS), that included high-resolution time-of-flight mass spectrometers. Only the measurements from the PTR-TOF-MS, operated by the National Oceanic and Atmospheric Administration, are used here. The PTR-TOF-MS measurements are described in detail in (Koss et al., 2018) and (Sekimoto et al., 2018). In addition to the NMOG measurements, other inorganic gases (O_3, CO, CO_2, SO_2) were measured using commercial instrumentation.

10.2 Supplemental Figures & Tables

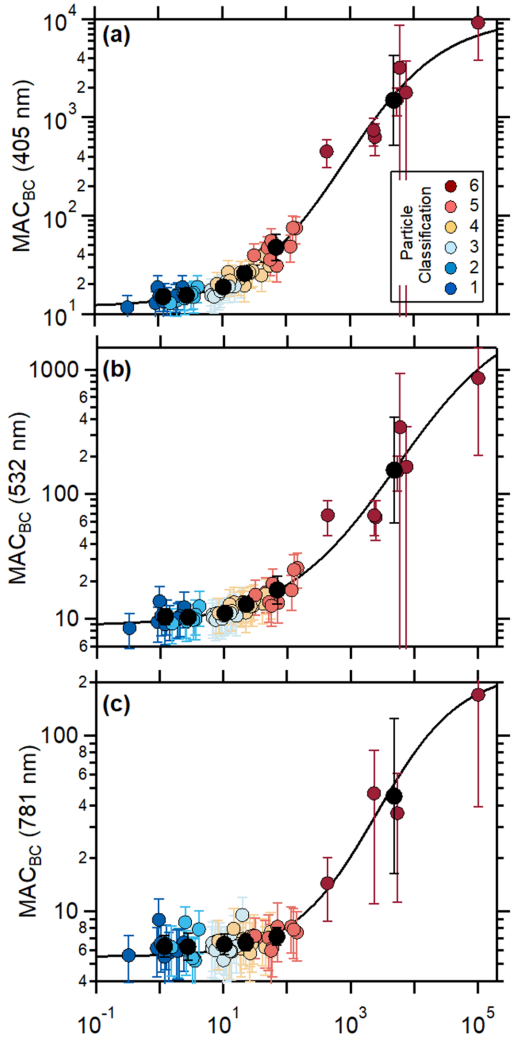

Figure S1. Relationship between the observed ambient particle MAC_{BC} and the total particle [OA]/[rBC] at (a) 405 nm, (b) 532 nm, and (c) 781 nm. Individual points colored by Class (see text) and class averages as black circles.

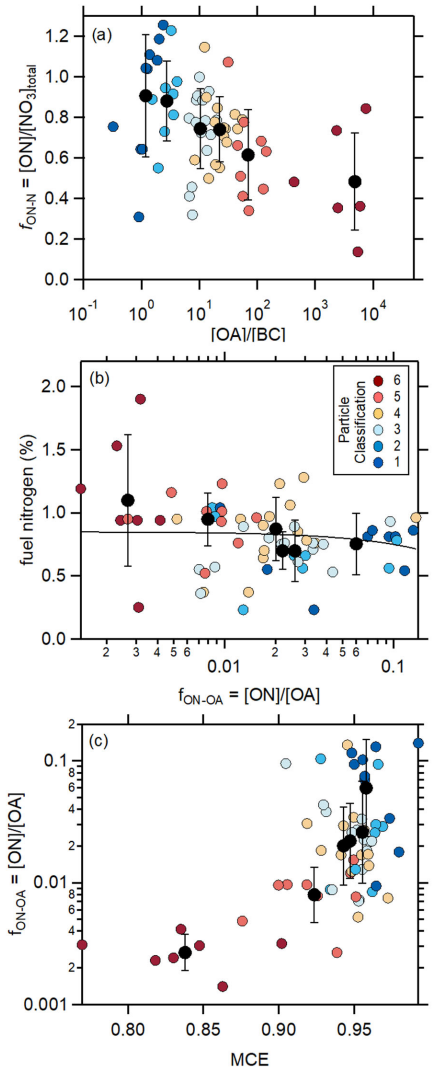

Figure S2. (a) Relationship between fuel nitrogen and the fraction of OA that is organic nitrate, f_{ON-N}. There is no correlation between the two. (b) Relationship between f_{ON-OA} and the modified combustion efficiency, MCE. Results for individual burns are shown as points colored by the particle Class, and Class average values are shown as black circles. Uncertainties on the Class averages are 1σ based on measurement variability.

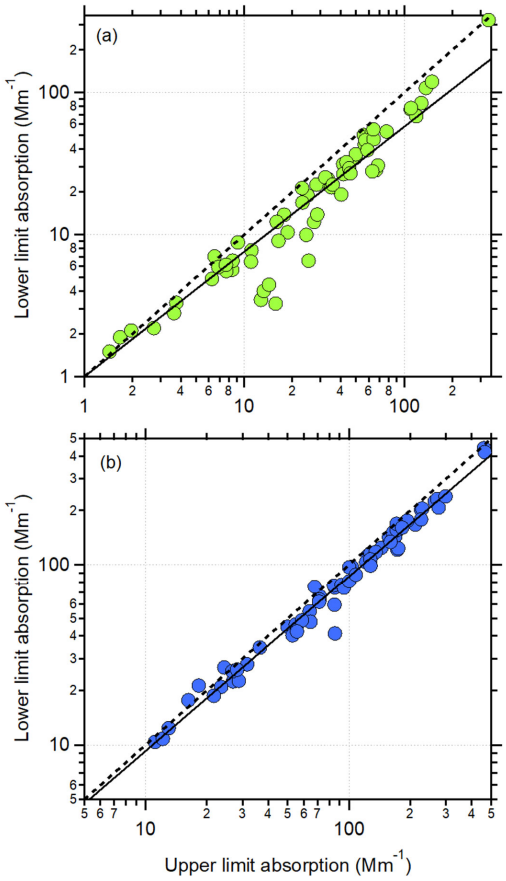

Figure S3. The derived lower limit brown carbon absorption versus the upper limit brown carbon absorption at (a) 532 nm and (b) 405 nm. The lower limit estimate for BrC absorption accounts for the potential influence of coating-induced enhancements. The dashed line is the one-to-one line and the solid line is a linear fit with slopes equaling 0.88 at 532 nm and 0.97 at 405 nm.

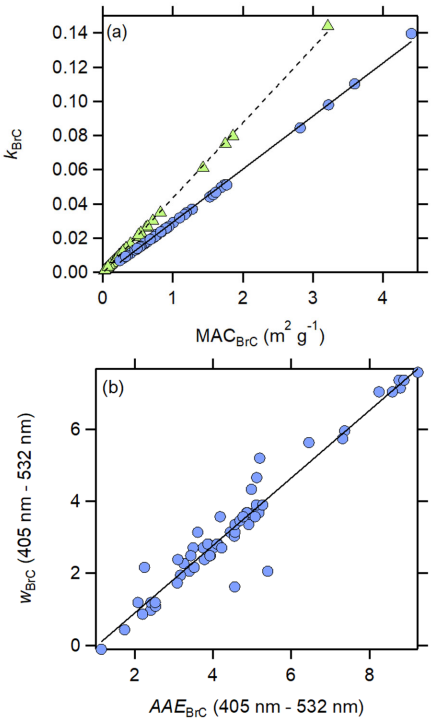

158

159 **Figure S4.** (a) Relationship between the imaginary refractive index for BrC, k_{BrC}, at 405 nm (blue
160 circles) and the observed MAC_{BrC} at 405 nm or at 532 nm (green triangles). Lines are linear fits to
161 the observations. (b) Relationship between the wavelength dependence of k_{BrC}, w_{BrC}, determined
162 for the 405 nm – 532 nm pair, and the AAE_{BrC} for the same wavelengths.
163

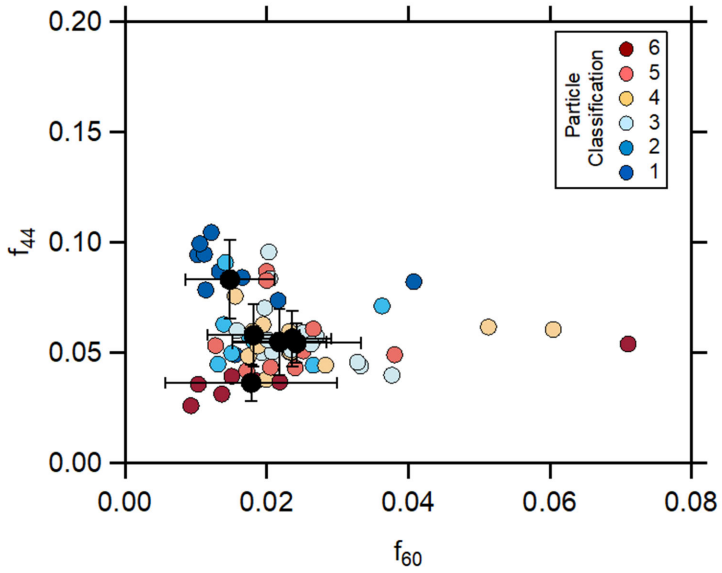

Figure S5. The relationship between the fractional abundance of the m/z = 44 (f_{44}) and m/z = 60 (f_{60}) ions from organic aerosol. Points are colored by particle class for individual burns, and the class averages shown in black.

Table S1. Fuels combusted. Further details regarding fuel properties are available at the NOAA data repository, in particular in the summary spreadsheet (https://esrl.noaa.gov/csd/groups/csd7/measurements/2016firex/FireLab/DataDownload/FIREX_BurnListComplete_V5.xlsx; access date 04 February 2019)

Fuel Type
Bear Grass
Building Material - Untreated Wood
Ceanothos
Chapparral (canopy)
Chamise
Manzanita
Douglas Fir (litter, canopy, mixture, rotten log)
Dung
Engelmann spruce (canopy, mixture, duff)
Excelsior (wood wool)
Jeffrey Pine (duff)
Juniper (canopy)
Loblolly pine (litter)
Lodgepole (canopy, litter, mixture)
Peat
Ponderosa pine (litter, canopy, mixture, rotten log)
Rice Straw, Arkansas
Sage
Sage Brush
Subalpine fir (canopy, litter, mix, duff)

Table S2. Fit coefficients for the various fits performed, organized by fit type (e.g. sigmoidal, power law, linear, exponential). Note: continues on second page.

y	x	c_1	c_2	c_3	c_4	r^2
		$y = c_1 + \frac{c_2}{1 + \frac{\exp(c_3 - x)}{c_4}}$				
SSA_{405nm}	log([OA]/[BC])	0.03	0.93	0.444	0.579	
SSA_{532nm}	log([OA]/[BC])	0.085	0.91	0.623	0.520	
SSA_{781nm}	log([OA]/[BC])	0.10	0.90	0.700	0.538	
$AAE_{405\text{-}532}$	log([OA]/[BC])	1.25	7.81	2.298	0.554	
$\log(MAC_{BC,405nm})$	log([OA]/[BC])	1.072	2.94	2.914	0.765	
$\log(MAC_{BC,532nm})$	log([OA]/[BC])	0.94	2.56	3.721	0.900	
$\log(MAC_{BC,781nm})$	log([OA]/[BC])	0.74	1.62	3.411	0.655	
$\log(f_{OA,int})$	log([OA]/[BC])	0	-2.43	1.477	0.987	
$\log(R_{OA,BC})$	log([OA]/[BC])	-1.76	3.70	0.462	1.823	
$\log(MAC_{BrC,405nm})$	log([OA]/[BC])	1.072	-1.519	0.053	0.732	
AAE_{405nm}	MCE	9.124	-7.476	0.884	0.0236	
AAE_{405nm}	MCE*	9.723	-13.142	0.932	0.0452	
$\log(MAC_{BC,405nm})$	MCE	3.523	-2.251	0.874	0.0198	
$\log(MAC_{BC,405nm})$	MCE*	4.949	-5.073	0.882	0.0705	
log([OA]/[BC])	MCE*	4.030	-39.57	1.072	0.0500	
		$y = c_1 + c_2 \cdot x^{c_3}$				
SSA_{405nm}	MCE	0.954	-0.880	22.76		
SSA_{405nm}	MCE*	0.939	-26.34	88.29		
log([OA]/[BC])	MCE	7.952	-8.272	3.351		
		$y = c_1 \cdot x + c_2$				
f_{44}	log([OA]/[BC])	-0.0097	0.0686			0.33
O:C	log([OA]/[BC])	-0.0345	0.407			0.17
H:C	log([OA]/[BC])	0.0228	1.737			0.27
$\log(MAC_{BrC,405nm})$	$\log(f_{ON\text{-}OA})$	0.322	0.446			0.33
$\log(MAC_{BrC,405nm})$	$\log(f_{ON\text{-}OA})^*$	0.856	0.538			0.81
$\log(MAC_{BrC,405nm})$	f_{60}/f_{44}	-0.396	0.043			0.11
$\log(MAC_{BrC,405nm})$	f_{60}/f_{44}^*	-2.242	0.803			0.96
log([ON]/[OA])	log([OA]/[BC])	-1.342	-0.320			0.47
log([ON]/[OA])	log([OA]/[BC])*	-1.342	-0.320			0.47
$k_{BrC,405nm}$	$MAC_{BrC,405nm}$	0.03104	-0.00177			0.99
$k_{BrC,532nm}$	$MAC_{BrC,532nm}$	0.0440	-0.00048			0.99

y	x	c_1	c_2	c_3	c_4	r^2
$w_{BrC,405-532}$	$AAE_{BrC,405-532}$	0.938	0.976			0.96
	$y = c_1 + c_2 \cdot \exp(-c_3 \cdot x)$					
MFR_{OA}	log([OA]/[BC])	0.00175	0.1760	0.8520		0.157

* Fits were performed to the Class averages, rather than to the individual burns.

178

179

Table S3. Literature imaginary refractive index and *MAC* values for biomass burning derived brown carbon.

	λ , nm	k_{BBOA}	MAC_{BBOA} $m^2 g^{-1}$	Optical Measurement	Aerosol type sampled	Sampling Location or note	Literature
Laboratory	550	0.02-0.06		Aethalometer	Oak burning POA	-	(Saleh et al., 2013)
	550	0.015-0.04		Aethalometer	Pocosin Pine burning POA	-	(Saleh et al., 2013)
	550	0.0055-0.022		Aethalometer	Galberry burning POA	-	(Saleh et al., 2013)
	400	0.038	1.1	UV/Vis (filter methanol extracts)	Pine/Oak wood burning	-	(Chen and Bond, 2010)
	405	0.015		Photo-Acoustic Spectrometer	Tar balls from Ponderosa Pine Duff burning	-	(Chakrabarty et al., 2010)
	405	0.0076		Photo-Acoustic Spectrometer	Tar balls from Alaskan Duff burning	-	(Chakrabarty et al., 2010)
	550		0.8-3.2	CLAP	Tar balls from liquid tar (turkey oak)	-	(Hoffer et al., 2016)
	405	0.01	0.35	Photo-Acoustic Spectrometer	Alaskan Peat	-	(Sumlin et al., 2017)
	355, 405, 532, 1064	0.012, 0.0065, 0.0024, 0.0023		Photo-Acoustic Spectrometer	Alaskan & Indonesian Peat	central values reported here	(Sumlin et al., 2018)
	600/400 ratio		0.04	Water soluble organic carbon	Florida peat	Ratio between wavelengths reported	(Sengupta et al., 2018)
Ambient	404	0.01	1.0-1.1	Photo-Acoustic Spectrometer	Wild fire, near-source emission	Four Mile Canyon, Colorado	(Lack et al., 2012a)
	470		1.01	Aethalometer	Biomass burning influenced	Beijing, China	(Yang et al., 2009)
	400	0.112	2.9	Filter transmission	Wood burning and biomass smoke aerosols	Savanna	(Kirchstetter et al., 2004)
	532	0.0016-0.0019	0.029-0.031	Photo-Acoustic Spectrometer	HULIS from biomass burning aerosols	Amazon basin	(Hoffer et al., 2006)
	Broadband	0.05-0.07		Airborne lidar	Upwind of forest fires	Northern Canada	(Wandinger et al., 2002)
	Broadband	0.07±0.03/ 0.04±0.01		White light optical particle counter	Open fire/ Smoldering phase	Urban Rehovot, Israel	(Adler et al., 2011)
	405	0.037	0.79 or 1.22	Photo-Acoustic Spectrometer	Residential biomass burning influenced	Fresno, CA	(Zhang et al., 2016)
	405		0.84	Photo-Acoustic Spectrometer	Residential biomass burning influenced	Fresno, CA	(Cappa et al., 2019b)
	405		2.3	Aethelometer	Biomass burning influenced	Guangzhou, China	(Qin et al., 2018)
	365		0.32	Water soluble organic carbon	Plume intercept – closest point to fire	Western US	(Forrister et al., 2015)
	365		1.35	Water soluble organic carbon	Regional biomass burning	SE US	(Washenfelder et al., 2015)

405	0.037		Water soluble organic carbon	Regional	Kanpur, India	(Shamjad et al., 2016)
405		0.7-1.3	Water soluble organic carbon	Bonfire festival	Rehovot, Israel	(Bluvshtein et al., 2017)
405		0.6	Methanol soluble organic carbon	Prescribed burn	NW US	(Xie et al., 2017)
400, 600, 800	0.31, 0.26, 0.22		Electron loss	Asian outflow	Downwind of Asia	(Alexander et al., 2008)
800/400 ratio		0.26	Methanol soluble organic carbon	Ambient particles (ratio between wavelengths reported)	Athens, Georgia	(Phillips and Smith, 2017)
400, 550, 700	0.112, 0.030, 0.001		Acetone treatment + attenuation	African biomass burning	Southern Africa	(Kirchstetter et al., 2004)

182